Catena xxx (2016) xxx–xxx

Contents lists available at ScienceDirect

Catena

journal homepage: www.elsevier.com/locate/catena

The loess-palaeosol sequence of Datthausen, SW Germany: Characteristics, chronology, and implications for the use of the Lohne Soil as a marker soil

Daniela Sauer [a,*], Annette Kadereit [b], Peter Kühn [c], Michael Kösel [d], Christopher E. Miller [e], Taeko Shinonaga [f], Sebastian Kreutzer [g], Ludger Herrmann [h], Wolfgang Fleck [d], Britt M. Starkovich [e,i], Karl Stahr [h]

[a] Institute of Geography, University of Göttingen, Göttingen, Germany
[b] Heidelberg Luminescence Laboratory, Institute of Geography, University of Heidelberg, Germany
[c] Research Area Geography, Laboratory of Soil Science and Geoecology, University of Tübingen, Germany
[d] Regierungspräsidium Freiburg - Dept. 9, State Authority for Geology, Mineral Resources and Mining, Freiburg i. Br., Germany
[e] Institute for Archaeological Sciences, University of Tübingen, Germany
[f] Helmholtz Zentrum München, German Research Center for Environmental Health, Institute of Radiation Protection, Neuherberg, Germany
[g] IRAMAT-CRP2A, Université Bordeaux Montaigne, Maison de l'Archéologie, Pessac, France
[h] Institute of Soil Science and Land Evaluation, University of Hohenheim, Stuttgart, Germany
[i] Senckenberg Center for Human Evolution and Palaeoenvironment (HEP), Tübingen, Germany

ARTICLE INFO

Article history:
Received 26 October 2015
Received in revised form 12 June 2016
Accepted 14 June 2016
Available online xxxx

Keywords:
Loess-palaeosol sequence
Middle to Upper Pleniglacial boundary
MIS3/MIS2 boundary
Lohne soil
Pedostratigraphic marker
Chronometric marker

ABSTRACT

A new loess-palaeosol sequence from the westernmost loess area along the upper Danube River in SW Germany is presented. The profile Datthausen comprises a sequence of Middle Pleniglacial (MPG) and Upper Pleniglacial (UPG) palaeosols, separated by a prominent erosional discontinuity. The uppermost MPG palaeosol consists of two olive-brown horizons, showing morphological characteristics of the "Lohne Soil" that represents the uppermost MPG palaeosol in many loess-palaeosol profiles in the humid loess regions of central Europe. Sedimentological, palaeopedological and micromorphological analyses, combined with luminescence dating, were carried out. Compared to the profiles Nussloch and Schwalbenberg II in the Rhine River region, the profile Datthausen shows more intense pedogenesis, mainly due to its position in a depression and lower loess-accumulation rates. Further, the MPG/UPG transition at Datthausen seems to date later in time, likely matching Greenland interstadial (GIS) 4 and/or GIS 3, rather than GIS 7 to GIS 5. We conclude that the Lohne Soil is a reliable pedostratigraphic marker, whereas its use as a chronometric marker *sensu stricto* (which should have formed during one well-defined phase of soil formation) is impeded as it evolved during several interstadials. Its use as a chronometric marker *sensu lato* (which may have formed over several phases of soil formation) is impeded, too, as its chronological position in different loess-palaeosol profiles may not be specific enough. The differences in pedogenesis and chronology between the profiles Nussloch and Schwalbenberg II on one side and the profile Datthausen on the other side are attributed to site-specific factors such as topography. The influence of these factors on pedogenesis at the local scale may prevail over the general climatic regime controlling soil formation at the regional level. Therefore, spatial diversity of palaeosols needs to be considered when matching loess-palaeosol profiles with marine and ice-core records for evaluating the impact of climate forcing on terrestrial palaeoenvironments.

© 2016 Elsevier B.V. All rights reserved.

1. Introduction

Research on loess-palaeosol sequences for reconstructing terrestrial palaeo-environments during Pleistocene glacial-interglacial cycles has a long tradition in Europe (e.g., Brunnacker, 1954; Fink, 1956; Semmel, 1969; Bibus, 1974; Haeserts, 1985; Pécsi and Richter, 1996; Smalley et al., 2001; Marković et al., 2009; Hambach et al., 2015). Over the last decades the interest in these palaeo-environmental archives has increased due to the expected global climatic change and the need for a deeper understanding of the impact of climate forcing on terrestrial environments (e.g., Rousseau et al., 2009, 2013). Mainly, loess-palaeosol sequences predominantly built up from primary aeolian loess were investigated (e.g., Antoine et al., 2001, 2009; Schirmer, 2012; Kreutzer et al., 2012a; Fuchs et al., 2013). The profile Datthausen provides additional insights from reworked loess deposits with several intercalated palaeosols. This sediment-palaeosol sequence sits on top of a penultimate glacial terrace of the Danube River which is exposed in the gravel quarry of Datthausen, in the westernmost known loess area along the upper Danube River in SW-Germany (Fig. 1).

* Corresponding author.
E-mail address: daniela.sauer@geo.uni-goettingen.de (D. Sauer).

http://dx.doi.org/10.1016/j.catena.2016.06.024
0341-8162/© 2016 Elsevier B.V. All rights reserved.

Please cite this article as: Sauer, D., et al., The loess-palaeosol sequence of Datthausen, SW Germany: Characteristics, chronology, and implications for the use of the Lohne Soi..., Catena (2016), http://dx.doi.org/10.1016/j.catena.2016.06.024

ARTICLE IN PRESS

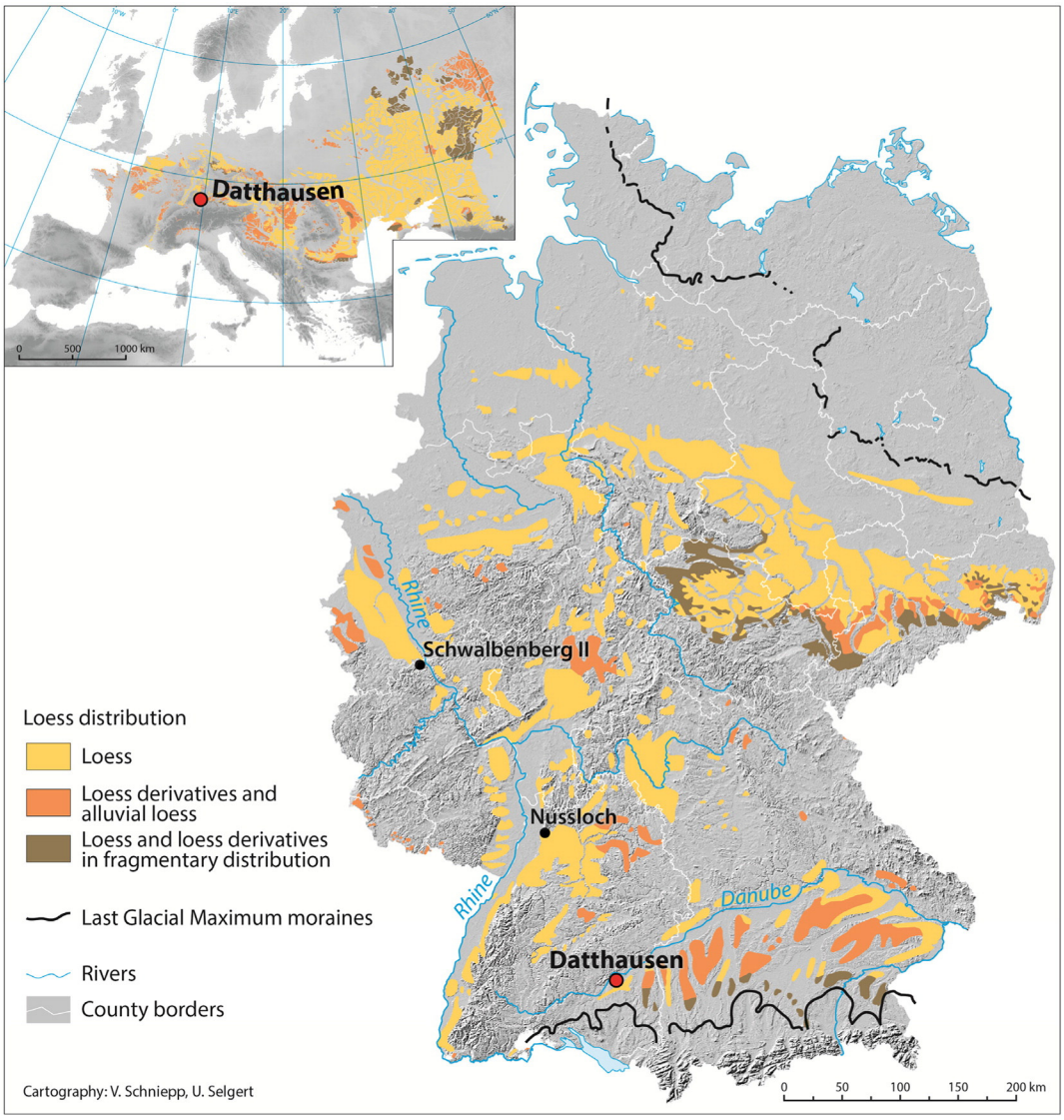


Fig. 1. Location of the loess-palaeosol sequence of Datthausen within the European loess belt and within Germany. Datthausen is situated in the westernmost known loess area along the upper Danube River in southwestern Germany. The loess distribution shown is from the map of Haase et al. (2007), applying the simplified classification after Kadereit et al. (2013), the digital terrain model is based on SRTM data (USGS, 2015).

The profile Datthausen was considered of special interest, as field observations suggested that it contains the transition from the terrestrial Middle Pleniglacial (MPG) to the Upper Pleniglacial (UPG) of the last glacial period (Middle Würmian to Upper Würmian in the stratigraphy of the northern Alpine foreland). The MPG parts of western and central European loess-palaeosol sequences are usually characterised by brownish subsoil remnants of Calcaric Brunic Regosols and transitions to Cambisols according to WRB (IUSS Working Group WRB, 2014) that formed during interstadials, whereas the UPG parts are characterised by less intensively developed palaeosols that formed under colder palaeoenvironmental conditions, such as Cryosols (Schönhals et al., 1964). In many loess-palaeosol sequences of western Germany, the uppermost MPG soil exhibits fine platy structure, an olive tint, and 1–2 mm size manganese and iron concretions in its upper, somewhat paler, part (Semmel, 2009). This palaeosol is called "Lohne Soil" in western Germany and adjacent regions because it was first described at a type locality near Lohne in Hesse, central western Germany (Schönhals et al., 1964). Typically, the MPG and UPG parts of loess profiles in western Germany are separated by a prominent erosional discordance immediately above the Lohne Soil (Semmel, 1969, 1995). Thus, the Lohne Soil is commonly regarded as a pedostratigraphic marker horizon indicating the MPG/UPG-transition (e.g., Schönhals et al., 1964; Semmel, 1995; Terhorst et al., 2001; Wagner, 2011; Zöller and Semmel, 2001). It serves for pedostratigraphic correlations from local to supra-regional scale with, e.g., the "Sinzig Soil 3" at Schwalbenberg II in western Germany (Schirmer, 2012); the "Vytachiv Soil" at Stayky in Ukraine (Rousseau et al., 2011); the "Bryansk Soil" in Russia (Pécsi and Richter, 1996; Rusakov and Sedov, 2012); "PK I" in the Czech Republic (Zöller et al., 1994; Frechen et al., 1999); and "Stillfried B" in the dry loess province of Lower Austria (Peticzka et al., 2010; Zöller et al., 2013; Terhorst et al., 2015). Therefore, here we also examine whether the profile Datthausen confirms the Lohne Soil as a reliable marker horizon. In this respect we consider it important to distinguish between a *pedostratigraphic* and a *chronometric marker*. A *pedostratigraphic marker* should exhibit a distinctive combination of characteristics. If these are macroscopically visible, the *pedostratigraphic marker* provides valuable orientation for field work. As a palaeosol reflects the environmental conditions at the time of soil formation, a *pedostratigraphic marker* has only limited spatial extent. The extent of the Lohne Soil is confined to the humid loess province of

Please cite this article as: Sauer, D., et al., The loess-palaeosol sequence of Datthausen, SW Germany: Characteristics, chronology, and implications for the use of the Lohne Soi..., Catena (2016), http://dx.doi.org/10.1016/j.catena.2016.06.024

Europe. Here it was reported from Mons (Belgium) and Lisieux (Normandy, France) in the west to Feilendorf (ca. 60 km West of Vienna, Austria) in the East (Bibus and Semmel, 1977; Semmel, 1995).

A *chronometric marker* should have been dated at several key profiles, resulting in a consistent chronometric position (e.g., the tephra of the Laach Lake eruption 12,900 a BP). The chronometric position of the Lohne Soil, and thus the timing of the terrestrial MPG/UPG transition, has recently become a matter of debate as an earlier suggested correlation with Greenland interstadial (GIS) 8 (e.g. Rousseau et al., 2011) appears questionable (Kadereit et al., 2013). In the loess profiles at Nussloch and Schwalbenberg II in western Germany, the Lohne soil appears to match the Denekamp interstadial (van der Hammen et al., 1967, 1995) of the western European terrestrial chronology (cf. Litt et al., 2007). The Denekamp interstadial in turn matches the time span (^{14}C-data from van Huissteden, 1990; van der Hammen, 1995) covering GIS 7 to GIS 5 of the Greenland ice core chronology CICC05 (Andersen et al., 2006; Svensson et al., 2006). GIS 7 to GIS 5 in turn fall into marine isotope stage (MIS) 3 (cf. stack of records by Lisiecki and Raymo, 2005). Thus, the Lohne Soil still seems to match the Denekamp interstadial, but neither the Denekamp nor the Lohne Soil match with GIS 8 as assumed earlier (for further details cf. Kadereit et al., 2013; Kadereit and Wagner, 2014 and literature quoted therein). However, a reliable chronology and matching of the terrestrial archives with the marine and ice core records is an essential requirement to understand the role of climatic forcing for terrestrial environments under global change.

The profile Datthausen exhibits a truncated MPG part which, below a prominent erosional discontinuity, terminates with a brownish palaeosol having Lohne Soil habitus. Thus, it offers the opportunity to contribute to the identification of the chronometric position of the Lohne Soil with new numeric datings and to evaluate the suitability of the Lohne Soil as a marker horizon. Therefore, here we present the sedimentological and palaeopedological characteristics of the profile, supported by grain size distribution data, soil chemistry, micromorphology and optically stimulated luminescence (OSL) dating. On this basis, the suitability of the Lohne Soil as a *pedostratigraphic* and *chronometric marker* is discussed.

2. Study site

2.1. Landscape setting

The loess-palaeosol profile Datthausen is located in a gravel quarry on a penultimate-glacial terrace of the Danube River in the south-western Alpine foreland (Fig. S-1.1 in Supplementary material 1). It is situated ca. 40 km SW of Ulm, near the boundary between the Alpine Molasse Basin and the Jurassic of Swabia.

During glacial periods the Danube River was a major drainage line for both meltwaters from the Rhine glacier that expanded from the Alps into the Alpine foreland, and meltwaters from the local ice cap of the southern Black Forest (cf. Graul, 1952). During the multiphase penultimate-glacial period (Rissian) the Rhine glacier advanced even beyond the present course of the Danube River in the western Alpine foreland. The ice lobe that extended farthest to the North accumulated a terminal moraine ca. 1.5 km southwest of the profile Datthausen. Meltwaters deposited shallow outwash fans north of the terminal moraine ridge. These fans open out into a coarse-grained sandur plain that in turn merges into the penultimate-glacial terrace of the Danube River (Geyer et al., 2011). The loess-palaeosol sequence of Datthausen sits on top of the gravel body of this terrace, in which the subsoil of a reddish brown Eemian Luvisol is preserved.

During the last glacial period the Rhine glacier expanded northwards, up to ca. 20 km south of the profile Datthausen. Glacial meltwaters ponded between the last-glacial ice margin and the penultimate-glacial terminal moraine further north, before the water discharged to the Danube River via the Riss River and other Danube tributaries. Each year, after the summer flushing of meltwaters had ceased, the bed of the Danube River became dry. Fine particles were blown out from the freshly deposited glaciofluvial sediments by the prevailing westerlies and the anticyclone winds over the Alpine ice sheet. Loess formed where the blown-out dust settled.

The present-day annual precipitation in the region is 812 mm (Gutenzell), and the mean annual temperature is 7.6 °C (Biberach) (Kösel, 2010). Under these climatic conditions, Luvisols represent the dominating soils on loess (Fig. S-1.2 in Supplementary material 1).

2.2. Loess-palaeosol sequence

In the eastern wall of the gravel quarry Datthausen a flat last-glacial channel within the penultimate-glacial terrace gravel was cut almost perpendicular to the course of the quarry works, thus exposing the last-glacial sediment-palaeosol infilling. Outside the channel, the loess cover is much shallower. The profile was described in the central part of the channel, where 4.7 m of – mainly reworked – loess has accumulated (Fig. 2). The sediment-palaeosol sequence below the present-day Luvisol is divided into a Middle Pleniglacial (MPG) and an Upper Pleniglacial (UPG) part. The MPG part is dominated by a sequence of intense brown palaeosol horizons, whereas the UPG part is characterised by two brown palaeosol horizons at its bottom, overlain by two weakly developed hydromorphic palaeosol horizons.

In detail, the loess-palaeosol sequence starts on top of an eroded reddish-brown Luvisol which is developed in the penultimate-glacial Danube gravel and thus interpreted as Eemian palaeosol. No early last-glacial palaeosols are preserved. The basal part of the profile,

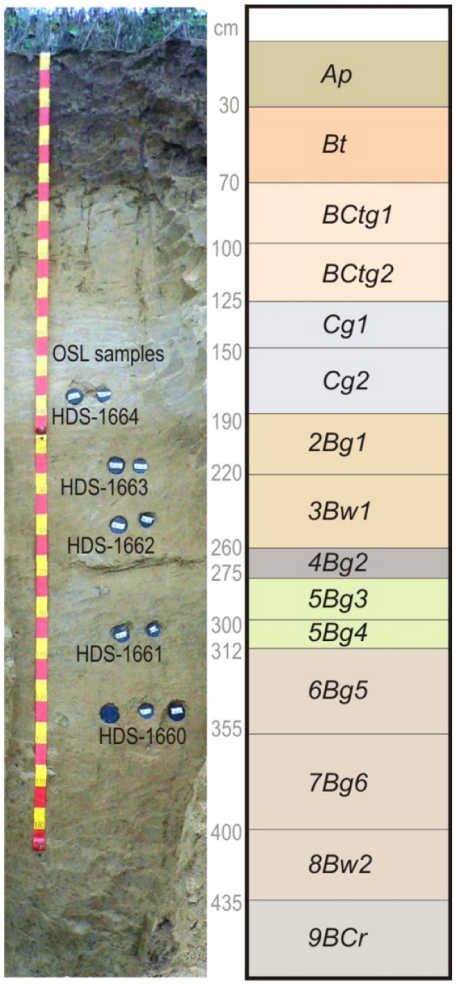


Fig. 2. Photo of the profile with positions of luminescence samples (left) and general scheme of the profile (right).

Please cite this article as: Sauer, D., et al., The loess-palaeosol sequence of Datthausen, SW Germany: Characteristics, chronology, and implications for the use of the Lohne Soi..., Catena (2016), http://dx.doi.org/10.1016/j.catena.2016.06.024

Table 1
Field description of the loess-palaeosol sequence Datthausen.

Depth [cm]	Horizon (FAO, 2006)	Coarse fragm.	Texture (FAO)	Colour (dry, moist) and major characteristics	Structure
-30	Ap	n. d.	n. d.	n. d.	n. d.
-70	Bt	none	SiL	10YR5/6 (yellowish brown), 10YR4/6 (dark yellowish brown); numerous earthworm channels and abundant dark brown clay coatings	angular blocky and prismatic; earthworm faeces
-100	BCtg1	none	SiL	10YR7/4 (very pale brown), 10YR5/4 (yellowish brown); slightly mottled; rusty and bleached spots, very fine Mn nodules; clay coatings in earthworm channels	massive; pinholes
-125	BCtg2	none	SiL	10YR6/4 (light yellowish brown), 10YR4/4 (dark yellowish brown); slightly mottled, fine Mn nodules; clay coatings in earthworm channels	massive; pinholes
-150	Cg1	none	SiL	2.5Y7/4 (pale brown), 2.5Y5/4 (light olive brown); very fine rusty spots and Mn nodules	massive, layered (fine sandy layers)
-190 *OSL:*	Cg2 *HDS-1664*	none	SiL	2.5Y7/3 (pale brown), 2.5Y5/4 (light olive brown); mottled, fine rusty spots (2 mm)	massive, layered (fine sandy layers)
-220 *OSL:*	2Bg1 *HDS-1663*	very few fine gravel	SiL	10YR6/4 (light yellowish brown), 10YR4/4 (dark yellowish brown); intense brown, slightly mottled	massive to weakly fine platy; pinholes
-260 *OSL:*	3Bw1 *HDS-1662*	very few fine gravel	SiL	10YR6/4 (light yellowish brown), 10YR5/4 (yellowish brown); snail shell fragments	massive to weakly fine platy; pinholes
-275	4Bg2	layer of fine + med gravel	SiL	10YR6/4 (light yellowish brown), 10YR5/4 (yellowish brown); slightly mottled	massive to weakly fine platy; pinholes
-300 *OSL:*	5Bg3 *HDS-1661*	none	SiL	10YR6/4 (light yellowish brown), 10YR5/4 (yellowish brown); very fine Fe+Mn mottles (2mm); slight olive tint; appearance similar to late MIS 3 "Lohne Soil"	massive to weakly fine platy; pinholes
-312	Bg4	none	SiL	10YR6/4 (light yellowish brown), 10YR4/4 (dark yellowish brown); slight olive tint; very fine Fe mottles and Mn nodules (2mm)	massive to weakly fine platy
-355 *OSL:*	6Bg5 *HDS-1660*	none	L	10YR6/4 (light yellowish brown), 10YR4/6 (dark yellowish brown) intense brown, somewhat more reddish than overlying horizons; fine soft Mn nodules	massive to weakly fine platy
-400	7Bg6	none	SiL	10YR6/4 (light yellowish brown), 10YR4/4 (dark yellowish brown); sparse Mn mottles and coatings	weakly fine platy and subangular blocky (1-2 cm); pinholes
-435	8Bw2	few fine + med gravel	SiL	10YR6/4 (light yellowish brown), 10YR4/4 (dark yellowish brown)	weakly subangular blocky; pinholes
-465	9BCr	medium + coarse gravel	CL	2.5Y7/4 (pale brown), 2.5Y5/4 (light olive brown); grayish; bleached and rusty mottles	weakly subangular blocky

representing the MPG, begins with a 30 cm thick pale greyish-brown palaeosol horizon, reflecting wet conditions (9BCr) that has a more clayey texture than all other horizons (Fig. S-1.3 in Supplementary material 1) and weak subangular blocky structure (Table 1). Some medium and coarse gravel that probably froze up from the underlying penultimate-glacial Danube terrace has been mixed into the material. This lowermost palaeosol horizon is not included in the interpretation of the sequence, because the wet conditions reflected in it are not related to any specific palaeo-environment but are due to the position of the profile in the deepest part of the channel.

Three intense yellowish-brown palaeosol horizons follow on top (8Bw2, 7Bg6, and 6Bg5). The lowermost of them (8Bw2) contains a little fine and medium gravel. The uppermost palaeosol of the MPG sequence comprises two brown soil horizons exhibiting a slight olive tint and fine platy structure (5Bg4 and 5Bg3). The upper one shows clear features of redox processes and reworking. It is somewhat paler

Please cite this article as: Sauer, D., et al., The loess-palaeosol sequence of Datthausen, SW Germany: Characteristics, chronology, and implications for the use of the Lohne Soi..., Catena (2016), http://dx.doi.org/10.1016/j.catena.2016.06.024

Table 2
OSL-samples and dose-rate data.

Lab. No.	Depth [cm]	Horizon (FAO)	Uranium [mg kg^{-1}]	Thorium [mg kg^{-1}]	Potassium [weight %]	Cosmic dose rate [Gy ka^{-1}]	Weight moist / weight dry (1)	Weight moist / weight dry (2)	Weight moist / weight dry (3)	Effective dose rate [Gy ka^{-1}]
HDS-1664	180	Cg2	2.86 ± 0.28	8.23 ± 0.49	1.28 ± 0.20	0.19 ± 0.02	1.10	1.10	1.10 ± 0.06	2.50 ± 0.22
HDS-1663	216	2Bg1	3.11 ± 0.30	9.74 ± 0.57	1.49 ± 0.23	0.20 ± 0.02	1.16	1.16	1.16 ± 0.06	2.68 ± 0.23
HDS-1662	245	3Bw1	3.11 ± 0.29	10.14 ± 0.60	1.48 ± 0.23	0.20 ± 0.02	1.18	1.17	1.18 ± 0.06	2.64 ± 0.22
HDS-1661	297	5Bg3	3.53 ± 0.37	11.71 ± 0.69	1.71 ± 0.26	0.20 ± 0.02	1.20	1.21	1.20 ± 0.06	2.95 ± 0.25
HDS-1660	333	6Bg5	3.45 ± 0.33	11.35 ± 0.69	1.59 ± 0.25	0.21 ± 0.02	1.19	1.20	1.20 ± 0.06	2.81 ± 0.24

(1) material from steel cylinders; (2) material sampled around the cylinder holes; (3) value used for age calculation.

and has 1–2 mm size manganese and iron concretions. Thus, these two soil horizons show all characteristics usually attributed to the Lohne Soil. A thin gravel band on top of the bipartite olive-brown soil marks the erosional discontinuity that separates the MPG and UPG parts. This band can be traced over ca. 170 m along the wall (4Bg2). It indicates that this erosional phase largely removed the MPG loess cover outside the channel and washed some gravel into the channel, before again loess accumulation set in during the UPG.

Above the gravel band two unusually intense brown, only slightly de-carbonated soil horizons (3Bw1 and 2Bg1) and two hydromorphic horizons (Cg2 and Cg1) follow. The top of the profile is made up of a present-day Luvisol comprising the horizon sequence Ap-Bt-BCtg1-BCtg2.

3. Materials and methods

3.1. Sedimentological and palaeopedological analyses

All horizons were sampled for particle size analyses and soil-chemical analyses by taking a mixed sample across the entire thickness of each horizon. Horizons thicker than 25 cm were subdivided. Undisturbed samples of selected horizons were taken for thin section preparation. Particle size analyses were done by the sieve and pipette method after removing carbonates by 10 % HCl. Total element contents were determined by X-ray fluorescence analysis, carbonate contents were analysed using a Scheibler apparatus. Soil organic carbon (SOC) contents were determined by analysing total carbon contents by CN elemental analyser and then subtracting carbonate carbon from total carbon. Contents of pedogenic oxides were determined by dithionite extraction (Mehra and Jackson, 1960), and contents of amorphous and poorly crystalline pedogenic oxides by oxalate extraction (Tamm, 1922, mod. by Schwertmann, 1964). Fe, Al and Mn were then measured in the extracts by atomic absorption spectrometry (AAS).

3.2. Optically stimulated luminescence dating

Two horizons below and three horizons above the prominent erosional discordance were selected for OSL dating (Fig. 2, Tables 1, 2). Dating was performed on coarse quartz grains (125–212 μm) applying a single aliquot regeneration (SAR) approach (Murray and Wintle, 2000) with small aliquots and blue-light stimulated luminescence (BLSL). With regard to the underlying geomorphic processes age-modeling was based on a combined finite-mixture (Galbraith, 2005) and minimum-age model approach (Galbraith et al., 1999).

3.2.1. Sampling

The samples were taken in November 2012 from a freshly cleaned profile wall. Samples were taken in light-proof steel cylinders that were hammered horizontally into the sediment (Fig. 2). Additional material was collected in plastic bags around the cylinder holes for dose-rate and water-content determination.

3.2.2. Sample preparation

The extraction of coarse quartz grain separates followed standard procedures (e.g. Kadereit et al., 2006). Samples were handled under subdued indirect red (ca. 660 nm) light conditions. The fine sand fraction of 125–212 μm was gained by wet sieving. Carbonates and organic matter were removed using acetic acid (20 %) and hydrogen peroxide (10 % and 30 %). The quartz fraction was gained by density separation in lithium polytungstate (2.74 g cm^{-3} > quartz ≥ 2.64 g cm^{-3}). The outer rim of the quartz grains, which might have been affected by external alpha radiation, was removed with hydrofluoric acid (48 %, 45 min). Elimination of potential fluorides after HF-etching was done by washing the separates in HCl (10 %, 30 min). Finally the fraction <90 μm was removed by sieving. Demineralized water was used for sieving and washing of the samples in between the various preparation steps. All samples showed slight infrared stimulated luminescence (IRSL) signals in a first round of measurements (32 aliquots each sample). Therefore, prior to a second round of measurements, the quartz separates of samples HDS-1660 to HDS-1663, of which enough material was left, were again density separated (3 × 2.64 g cm^{-3}), HF-etched (48 %, 10 min), and washed in HCl (10 %, 60 min). This time, the fraction <125 μm was removed by sieving. From sample HDS-1664 a new portion of sediment was subjected to a more rigorous preparation procedure including final dry sieving <125 μm. However, the additional treatment could not eliminate the slight IRSL signals. As the results of the measurements before and after the intensified sample preparation were consistent, the different data sets of a sample were treated as one.

Small aliquots of 300–400 grains each (cf. Fuchs, 2001; Müller, 2012) were produced for luminescence measurements. Grains were settled on aluminium cups (ø ca. 10 mm) using silicon oil and a hole-mask (ø ca. 4 mm). Although they may be beneficial for insufficiently bleached sediments, smaller aliquots were not used as test measurements showed only moderately bright luminescence signals (few 10^3 counts for ca. 95 Gy; see Fig. 6a).

Table 3
General scheme of the SAR protocol developed for dose equivalent (D_e) measurements of the Datthausen samples.

Set	Run 1	Run 2–Run 9	Run 10[b]
1		Beta regeneration[a]	Beta 700 s
2	PHT 10 s @ 240 °C	PHT 10 s @ 240 °C	PHT 10 s @ 240 °C
3	Pause 0 s	Pause 0 s	IRSL 40 s @ 125 °C
4	BLSL 40 s @ 125 °C	BLSL 40 s @ 125 °C	BLSL 40 s @ 125 °C
5	Beta 700 s	Beta 700 s	Beta 700 s
6	Pause 0 s	Pause 0 s	Pause 0 s
7	TL/PHT 10 s @ 160 °C	TL/PHT 10 s @ 160 °C	TL/PHT 10 s @ 160 °C
8	BLSL 40 s @ 125 °C	BLSL 40 s @ 125 °C	BLSL 40 s @ 125 °C

[a] Beta = 200 s, 400 s, 700 s , 1000 s, 1300 s, 1600 s, 200 s (recycling-ratio test), 0 s (recuperation test); the beta-irradiation times correspond to ca. 19 Gy, 38 Gy, 67 Gy, 96 Gy, 124 Gy, 152 Gy, 19 Gy and 0 Gy.
[b] IRSL-test at 125 °C.

Please cite this article as: Sauer, D., et al., The loess-palaeosol sequence of Datthausen, SW Germany: Characteristics, chronology, and implications for the use of the Lohne Soi..., Catena (2016), http://dx.doi.org/10.1016/j.catena.2016.06.024

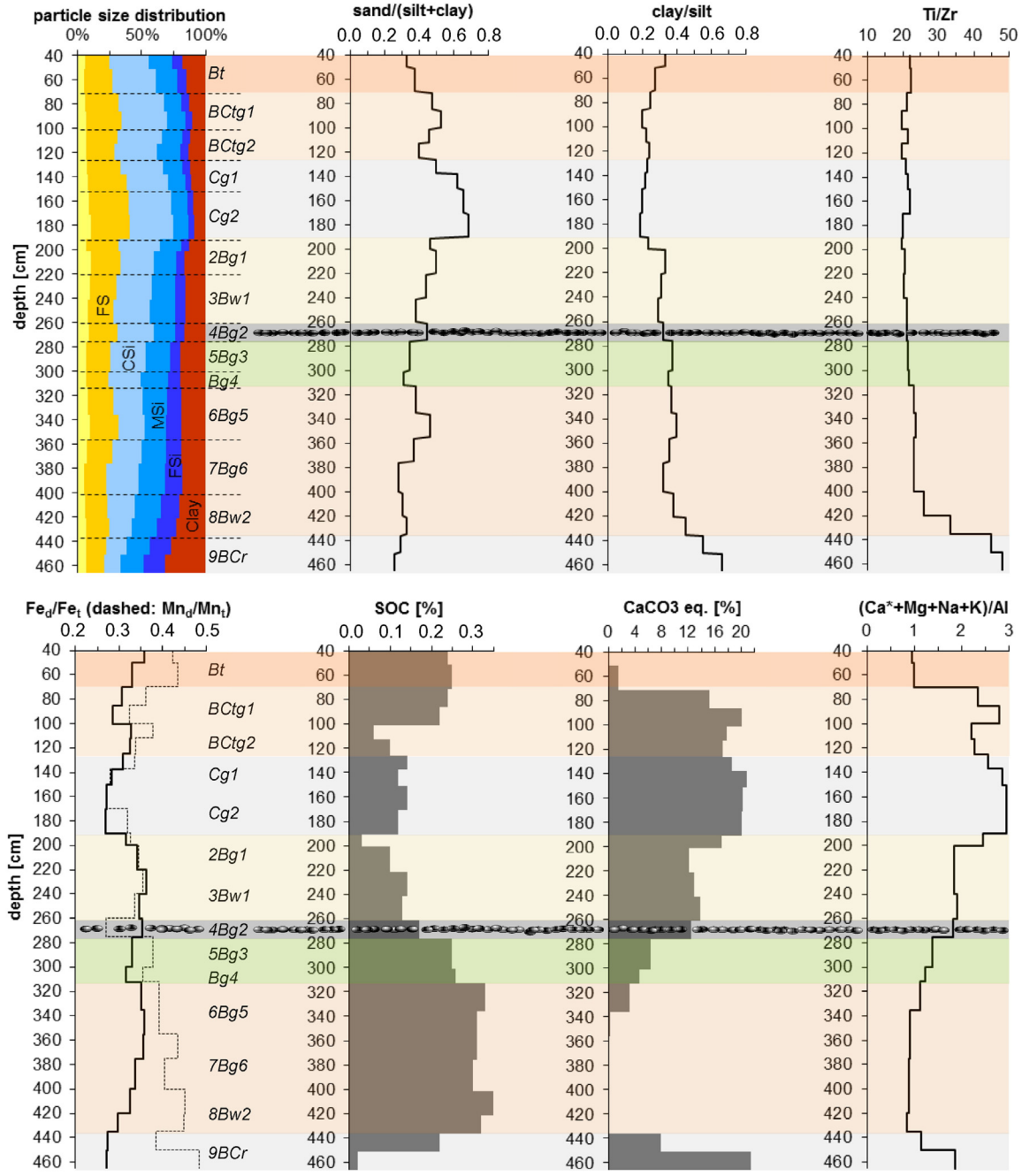


Fig. 3. Grain-size and soil-chemical data. The dark grey horizontal bar with pebble marks the gravel layer at the MPG/UPG (Middle/Upper Pleniglacial) boundary. The depth axes start at 40 cm, because the Ap horizon of the Holocene soil was not analysed.

3.2.3. Instrumentation

OSL measurements were carried out at the Heidelberg Luminescence Laboratory on an automated luminescence reader model TL/OSL Risø DA20 (DTU Nutech, 2015) equipped with four clusters of blue light emitting diodes (7 LEDs each; 470 nm Δ 20 nm) for blue light stimulated luminescence (BLSL), three clusters of infrared red emitting diodes (7 LEDs each; 870 nm) for infrared stimulated luminescence (IRSL), a bialkali photomultiplier tube (PMT) EMI 9235QB15 for signal detection, a calibrated $^{90}Sr/^{90}Y$ beta-source (ca. 5.7 Gy min^{-1} at the time of measurements) for laboratory irradiation, and a heater unit for thermal pre-treatment ('preheat') of the samples prior to BLSL readout. BLSL was measured for 40 s at 125 °C and detection of the quartz UV-signal occurred through a set of three glass filters U340 (2.5 mm each) in front of the PMT tube. BLSL readout was recorded in 250 data channels (0.16 s per data channel).

Thermal pre-treatment of the samples prior to BLSL readout may be performed either as an ordinary preheat (no data recording) or as thermally stimulated luminescence (thermoluminescence, TL), recording the data as a TL glow curve. The latter allows for controlling the heater unit during SAR measurement. The TL command permits to include preheat for a definite time. In a SAR protocol preheat-1 precedes the BLSL readout of a regeneration dose point and preheat-2 (also 'cutheat') precedes the BLSL readout within the normalisation dose (also 'test dose') sub-cycle. For the SAR measurements of the Datthausen samples we performed preheat-1 as an ordinary preheat at a particular temperature for 10 s duration, and preheat-2 as a TL run with a ramp of 5 °C s^{-1},

including a preheat of 10 s duration at a particular temperature. For technical reasons the TL exit temperature was 5 °C higher than the desired preheat temperature. Here we quote only the relevant preheat temperature kept in each case for 10 s duration (cf. Kadereit and Kreutzer, 2013).

3.2.4. SAR protocol

Based on a series of pre-tests (Section 2.2 in Supplementary material 2), we developed a SAR protocol as summarised in Table 3. BLSL readout occurred for 40 s at 125 °C. We administered a normalisation dose of ca. 67 Gy (700 s). Preheat-1 of 10 s at 240 °C was performed as an ordinary preheat, preheat-2 of 10 s at 160 °C was recorded as a TL glow curve. The natural BLSL signal was read out in run 1. The expected dose was ca. 1000 s (ca. 95 Gy; 100 %). Regeneration dose points (run 2 to run 9) were at 20 %, 40 %, 70 %, 100 %, 130 %, 160 %, 20 % (repetition of the smallest regeneration dose point to monitor how well the SAR procedure compensates sensitivity changes during a complete SAR measurement; so called 'recycling ratio') and 0 % (to check for any recuperation of the BLSL signal induced by the thermal pre-treatment; recuperation test). Finally in run 10, a regeneration dose of 700 s (70 % of the expected dose) was administered a second time followed by an IRSL readout at 125 °C (to scrutinise the sample for potential feldspar contamination; IRSL-test). Each SAR measurement was performed on 32 aliquots per sample, which lasted for ca. 8 days each. Each sample was measured twice in order to produce sufficient measurement results for reliable age determination.

3.2.5. Data analysis

Interpolating the natural luminescence signal of a sample onto a SAR growth curve (see Fig. 6c, f) allows for determining the equivalent dose (D_e) which corresponds to the sample's natural palaeodose. D_e determination occurred with the software program Analyst, Version 4.10 (Duller, 2013). SAR dose response curves were fitted with a single exponential model, considering 2 % measurement error to allow for potential over-dispersion of the PMT (cf. Adamiec et al., 2012), and including the error in the curve fitting. The following threshold criteria were applied: recycling ratio, maximum test dose error, maximum recuperation and maximum palaeodose error ≤10 %; BLSL signal >3 sigma above the background signal, and IRSL signal at 125 °C ≤10 % of the BLSL signal at 125 °C. D_e values from aliquots not meeting these quality criteria were eliminated from the data set prior to OSL-age calculation. In addition, aliquots were eliminated, for which the D_e had to be extrapolated beyond the highest SAR regeneration-dose point of 1600 s (ca. 150 Gy) which corresponds to ca. 50–60 ka for dose rates of ca. 2.5–2.9 Gy ka^{-1}.

Finite-mixture age analysis (Galbraith, 2005) and minimum-age analysis (Galbraith et al., 1999) were performed with the R package 'Luminescence' (version 0.3.4; Kreutzer et al., 2012b). Calculation of the OSL ages was done with an *Excel™* sheet (cf. Fuchs, 2001) using dose-conversion factors of Guérin et al. (2011).

3.2.6. Dose rate determination

Dose rate determination was done by low level gamma spectrometry which allows for detecting possible radioactive disequilibria in the uranium chain. Measurements were carried out at the Radioanalytical Laboratory, Helmholtz Centre Munich. The cosmic dose rate was calculated with the R package 'Luminescence' (Kreutzer et al., 2012b). As pore water diminishes the effective dose rates it has to be considered for OSL-age calculation. The water content of the luminescence samples was measured twice: once on the sediment in the cylinders that was taken off at both ends of the cylinders, because the sediment close to the ends of the cylinders might have been influenced by light during sample collection; and once on the surrounding sediment collected for gamma dose spectrometry. The measured values were taken as representative for the dating period considering an error of 0.06 (1 sigma, ratio of wet sample weight to dry sample weight; see Supplementary material 3 for further details).

4. Results

4.1. Textural, soil-chemical and micromorphological characteristics and their interpretation

4.1.1. Textural characteristics of the profile

The texture of almost the entire profile is predominated by coarse silt (CSi), followed by fine sand (FS) (Fig. 3). The texture tends to

Table 4
Particle size distribution data.

Depth [cm]	Horizon (FAO, 2006)	part	cS [wt.-%]	mS [wt.-%]	fS [wt.-%]	cSi [wt.-%]	mSi [wt.-%]	fSi [wt.-%]	Σ clay [wt.-%]	Σ silt [wt.-%]	Σ sand [wt.-%]
-50	Bt	upper	0.2	6.1	18.6	30.6	18.2	7.5	18.8	56.4	24.8
-70		lower	0.1	4.9	22.4	33.6	16.4	7.2	15.5	57.1	27.4
-85	BCtg1	upper	0.1	6.0	26.0	35.5	13.3	5.7	13.3	54.5	32.2
-100		lower	0.1	6.2	28.2	35.0	14.1	5.4	10.9	54.6	34.5
-112	BCtg2	upper	n. d.	n. d.	n. d.	n. d.	n. d.	n. d.	n. d.	n. d.	n. d.
-125		lower	0.1	6.9	21.4	33.8	17.5	6.6	13.7	57.9	28.4
-137	Cg1	upper	n. d.	n. d.	n. d.	n. d.	n. d.	n. d.	n. d.	n. d.	n. d.
-150		lower	0.1	7.9	30.4	32.5	13.3	4.8	11.0	50.6	38.4
-170	Cg2	upper	n. d.	n. d.	n. d.	n. d.	n. d.	n. d.	n. d.	n. d.	n. d.
-190		lower	0.0	10.3	30.4	33.9	11.9	4.3	9.1	50.1	40.8
-200	2Bg1	upper	0.1	6.6	24.9	32.3	16.6	6.4	13.0	55.4	31.6
-220		lower	0.4	10.2	22.7	26.3	16.8	6.8	16.7	50.0	33.3
-240	3Bw1	upper	n. d.	n. d.	n. d.	n. d.	n. d.	n. d.	n. d.	n. d.	n. d.
-260		lower	0.3	8.2	19.2	28.5	19.8	7.8	16.2	56.1	27.7
-275	4Bg2	whole	0.3	8.3	22.3	28.3	17.0	6.9	16.8	52.2	31.0
-300	5Bg3	whole	0.2	6.2	19.5	27.2	19.0	7.6	20.3	53.8	25.9
-312	5Bg4	whole	0.3	6.3	17.3	25.1	21.5	9.9	19.7	56.5	23.8
-335	6Bg5	upper	n. d.	n. d.	n. d.	n. d.	n. d.	n. d.	n. d.	n. d.	n. d.
-355	6Bg5	lower	0.4	9.4	21.8	21.0	16.5	11.4	19.4	48.9	31.7
-375	7Bg6	upper	n. d.	n. d.	n. d.	n. d.	n. d.	n. d.	n. d.	n. d.	n. d.
-400	7Bg6	lower	0.3	5.1	16.7	25.4	21.0	12.7	18.8	59.1	22.1
-420	8Bw2	upper	n. d.	n. d.	n. d.	n. d.	n. d.	n. d.	n. d.	n. d.	n. d.
-435	8Bw2	lower	0.6	6.2	17.9	17.5	19.4	15.1	23.3	52.0	24.7
-450	9BCr	upper	n. d.	n. d.	n. d.	n. d.	n. d.	n. d.	n. d.	n. d.	n. d.
-465	9BCr	lower	2.3	4.7	13.8	13.0	18.1	16.7	31.6	47.7	20.7

Please cite this article as: Sauer, D., et al., The loess-palaeosol sequence of Datthausen, SW Germany: Characteristics, chronology, and implications for the use of the Lohne Soi..., Catena (2016), http://dx.doi.org/10.1016/j.catena.2016.06.024

Table 5
Soil-chemical data.

Depth [cm]	Fe_t [g kg^{-1}]	Fe_d [g kg^{-1}]	Fe_o [g kg^{-1}]	Fe_d/Fe_t	Fe_o/Fe_d	Al_d [g kg^{-1}]	Al_o [g kg^{-1}]	Mn_d [g kg^{-1}]	Mn_o [g kg^{-1}]	$CaCO_3$ [eq. %]	SOC [%]
-50	31.16	11.19	1.60	0.36	0.14	0.99	0.82	0.43	0.41	0.16	0.24
-70	29.44	9.74	1.59	0.33	0.16	0.86	0.71	0.43	0.41	1.45	0.25
-85	21.15	6.46	0.90	0.31	0.14	0.47	0.39	0.31	0.20	15.2	0.24
-100	19.98	5.72	0.52	0.29	0.09	0.35	0.33	0.27	0.16	20.1	0.22
-112	22.27	7.29	0.62	0.33	0.09	0.46	0.41	0.33	0.21	17.8	0.06
-125	22.46	7.30	0.55	0.33	0.08	0.49	0.37	0.28	0.16	17.2	0.10
-137	20.69	6.39	0.50	0.31	0.08	0.41	0.30	0.27	0.13	18.5	0.14
-150	19.71	5.58	0.47	0.28	0.08	0.32	0.22	0.23	0.13	20.8	0.12
-170	18.57	5.02	0.34	0.27	0.07	0.31	0.24	0.22	0.13	20.3	0.14
-190	18.04	4.84	0.31	0.27	0.06	0.33	0.22	0.26	0.15	20.1	0.12
-200	20.52	6.48	0.42	0.32	0.06	0.44	0.30	0.28	0.22	17.1	0.03
-220	24.37	8.34	0.58	0.34	0.07	0.57	0.39	0.31	0.26	12.1	0.10
-240	24.73	8.95	0.51	0.36	0.06	0.59	0.37	0.29	0.22	12.9	0.14
-260	24.93	8.65	0.55	0.35	0.06	0.56	0.53	0.28	0.23	13.9	0.13
-275	23.95	8.45	0.61	0.35	0.07	0.61	0.51	0.23	0.23	12.4	0.17
-300	27.54	9.06	0.61	0.33	0.07	0.67	0.63	0.34	0.30	6.37	0.25
-312	29.53	9.34	0.80	0.32	0.09	0.72	0.71	0.31	0.27	4.69	0.26
-335	29.81	10.49	1.23	0.35	0.12	0.75	0.72	0.35	0.30	3.23	0.33
-355	29.63	10.63	1.54	0.36	0.15	0.75	0.81	0.34	0.31	0.19	0.31
-375	31.29	11.14	1.75	0.36	0.16	0.79	0.87	0.40	0.36	0.02	0.31
-400	32.21	10.89	1.56	0.34	0.14	0.80	0.86	0.42	0.42	0.04	0.30
-420	33.20	10.82	1.70	0.33	0.16	0.74	0.84	0.46	0.43	0.10	0.35
-435	35.80	10.61	1.57	0.30	0.15	0.73	0.77	0.40	0.35	0.05	0.32
-450	40.49	11.02	1.33	0.27	0.12	0.56	0.66	0.37	0.27	7.87	0.22
-465	35.70	9.68	1.20	0.27	0.12	0.46	0.46	0.54	0.42	21.4	0.02

become coarser from the bottom to the top of the profile. Coarse silt and fine sand make up 21–29 % (CSi) and 17–23 % (FS) of the material below 2 m depth. These values increase to 32–36 % (CSi) and 19–30 % (FS) in the upper 2 m of the profile. Such shift may be due to a change in the distance of the source of loess and/or wind velocity. Both explanations may apply to the profile Datthausen, as maximum sand contents occur between 140 cm and 190 cm depth (Fig. 3). This part of the profile corresponds to the time of maximum advance of glaciers, thus least distance to the source of dust and harshest environmental conditions. Especially the ratios of sand/(silt + clay) point out the maximum of coarsening at 140–190 cm depth very clearly, and moreover indicate two other secondary maxima at 335–355 cm and 85–100 cm depth (Fig. 3). However, caution is required in the interpretation of such minor maxima that include only thin layers. They may also be a result of preferential out-wash of fines by surface run-off leading to residual accumulation of coarser particles. Such process is not unlikely as most of the loess in this profile has been washed into the flat channel in which the profile is located, probably by surface run-off related to meltwaters that could not infiltrate into the frozen ground. It can be assumed that during those periods when sediment was washed into the channel, surface run-off occurred inside the channel as well, even concentrating there, leading to relative enrichment of sand in the channel. A minor sand/(silt + clay) maximum that is clearly related to a period of enhanced sheet-wash also occurs in the gravel band at 260–275 cm depth that separates the MPG and UPG parts of the profile. Some more sandy parts likewise occur in the loess-palaeosol sequence at Nussloch. There, they also have been attributed to sediment reworking or extraordinary strong winds that led to influx of coarser particles from the nearby alluvial plain of the Upper Rhine River, e.g., during the time of Heinrich events (Antoine et al., 2001, 2009).

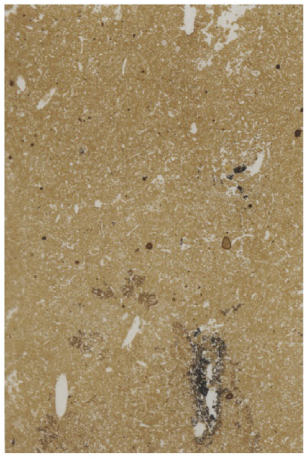
Clay contents in the profile Datthausen range between 16 % and 20 % in most of the profile; minimum clay contents of 9–14 % occur in the UPG part of the profile, at 70–200 cm depth (Table 4). Clay contents increase below 4 m depth to 23 % in the 8Bw2 and 32 % in the 9BCr horizon. This increase (also reflected in the clay/silt ratios in Fig. 3) is however not related to pedogenic clay formation but to an admixture of another sedimentological component. This admixture is indicated by the Ti/Zr ratios that show rather homogeneous values of 20–24 throughout the upper 4 m of the profile and an increase to 26–33 in the 8Bw2 and 44–48 in the 9BCr horizon.

4.1.2. Soil-chemical and micromorphological characteristics of the Middle Pleniglacial (MPG) palaeosol horizons

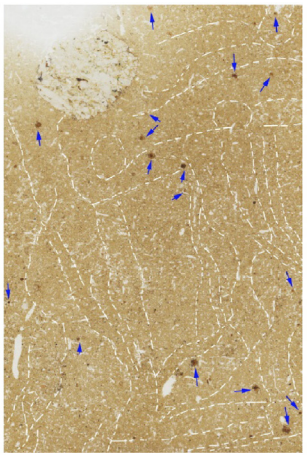
4.1.2.1. Soil-chemical characteristics. The soil-chemical data of the MPG palaeosol horizons (Fig. 3), especially their high Fe_d/Fe_t ratios, Mn_d/Mn_t ratios and soil organic carbon (SOC) contents, and their lower carbonate contents compared to the less weathered parts of the profile (Table 5), underline the rather intensive pedogenesis that is also expressed in the profile morphology and additionally confirmed by the weathering index based on the molar element ratio $(Ca^* + Mg + Na + K)/Al = WI_{MER}$, where Ca^* is the amount of Ca in aluminosilicates (calculated as total Ca minus Ca in Ca carbonate; the latter includes some uncertainty, because it is calculated based on the assumption that all carbonates measured by the Scheibler method is Ca carbonate; however, Mg carbonate most likely contributes, too). The WI_{MER} index reflects (most directly, compared to other weathering indices) release of Ca, Mg, Na and K from weathering aluminosilicates, and subsequent leaching of these elements and relative enrichment of Al which is immobile in the given environment (Sauer et al., 2010).

All MPG palaeosol horizons (275–435 cm depth; greenish and brownish colours in Fig. 3) show Fe_d/Fe_t ratios of 0.30–0.36; the max. Fe_d/Fe_t ratios of 0.35–0.36 are found in the horizons 6Bg5 and 7Bg6 (312–400 cm depth), characterised by the most intense brown colour. Their Fe_d/Fe_t ratios even equal those of the Bt horizon of the present-day surface soil (Fig. 3). All MPG palaeosol horizons show Mn_d/Mn_t ratios that are even higher than their Fe_d/Fe_t ratios (Fig. 3), amounting to 0.39–0.43 in the 6Bg5 and 7Bg6, compared to 0.42–0.43 in the present-day Bt horizon. These high Mn_d/Mn_t ratios match with abundant manganese mottles, nodules and coatings that are observed in almost all MPG palaeosol horizons. All MPG palaeosol horizons have SOC contents of 0.25–0.35 %, most of them thus exceeding those of the Bt horizon of the present-day surface soil (0.24–0.25 %). Also the clay/silt ratios of all MPG palaeosol horizons (0.32–0.40) are similar to those of the upper part of the Bt horizon of the modern Luvisol at 30–50 cm depth (0.33), indicating rather intense clay formation in these

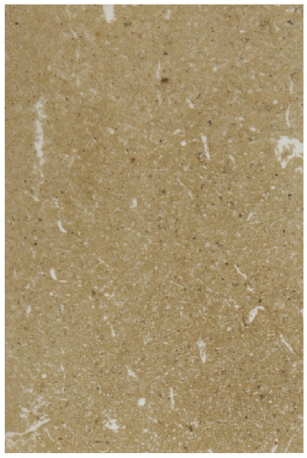
Please cite this article as: Sauer, D., et al., The loess-palaeosol sequence of Datthausen, SW Germany: Characteristics, chronology, and implications for the use of the Lohne Soi..., Catena (2016), http://dx.doi.org/10.1016/j.catena.2016.06.024



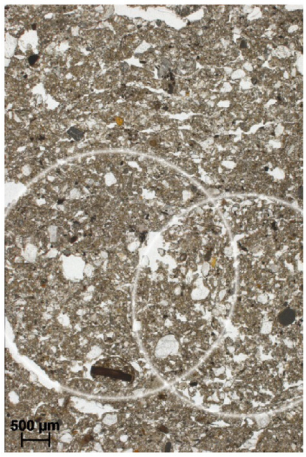
a) Photo of whole thin section (6 × 9 cm) of 6Bg5 (329-339 cm depth): Compacted granular to crumbly microstructure, channel microstructure and partly spongy microstructure. White areas mostly represent voids, namely vughs and channels. Dark brown roundish dots are different kinds of ferruginous, mostly concentric nodules. Passage features are detectable nearly everywhere.



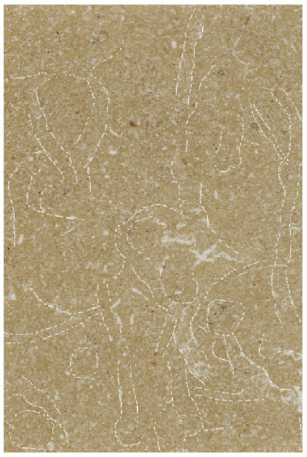
b) Photo of whole thin section (6 × 9 cm) of 5Bg4 (301-311 cm depth): Channel microstructure and more or less compacted crumbly to grain microstructure related to passage features. White areas are voids, namely vughs and channels. White broken lines mark passage features. There is a rounded fragment of sandstone with glauconite and carbonate (Ø ca. 3 cm) in the upper left corner. Blue arrows point to concentric to aggregate nodules.



c) Photo of whole thin section (6 × 9 cm) of 3Bw1 (230-240 cm depth): Lenticular platy microstructure and more or less compacted crumbly to grain microstructure. White areas represent voids, namely vughs, channels and few planes.



d) 3Bw1 (230-240 cm depth): The two white circles mark re-filled channels. Bioturbation has destroyed the original granular and lenticular structure that is still preserved above the two re-filled channels in the upper third of the microphotograph (plane polarised light).



e) Photo of whole thin section (6 × 9 cm) of 2Bg1 (202-212 cm depth): Weakly developed lenticular platy microstructure and more or less compacted crumbly microstructure. White areas represent voids, namely vughs, channels and few planes. Dashed white lines mark passage features.



f) Photo of whole thin section (6 × 9 cm) of Cg2 (163-173 cm depth): Lenticular platy microstructure. Dashed white lines mark passage features.

Fig. 4. Overview photographs of whole soil thin sections (except for4d which is a micro-photograph). (For interpretation of the references to colour in this figure, the reader is referred to the web version of this article.)

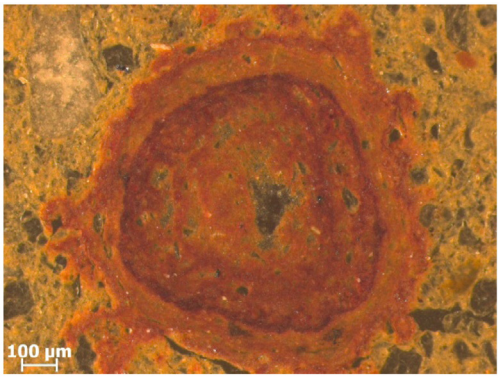
palaeosols. The considerably increasing clay/silt ratios below 4 m depth (8Bw2 and 9BCr) are however not related to pedogenic clay formation but to a sedimentological change as already mentioned in Section 4.1.1.

The palaeosol horizons 6Bg5, 7Bg6 and 8Bw2 (312–435 cm depth; brownish colour in Fig. 3) are completely decarbonated. The intense pedogenesis of these horizons is also reflected in their WI_{MER} values of 0.84–1.12, compared to 0.95–0.99 in the Bt horizon of the present-day surface soil. The overlying olive-brown soil horizons 5Bg3 and 5Bg4 that together form the uppermost MPG soil remnant exhibiting a characteristic Lohne Soil habitus (275–312 cm depth; greenish colour in Fig. 3), show slightly lower Fe_d/Fe_t ratios (0.32–0.33) and SOC contents (0.25–0.26 %) compared to the underlying intense brown-coloured horizons 6Bg5 and 7Bg6. The horizons 5Bg3 and 5Bg4 have 4.7–6.4 % calcium carbonate and WI_{MER} values of 1.2–1.4, confirming a slightly lower degree of weathering and element leaching compared to the underlying intense brown palaeosol horizons.

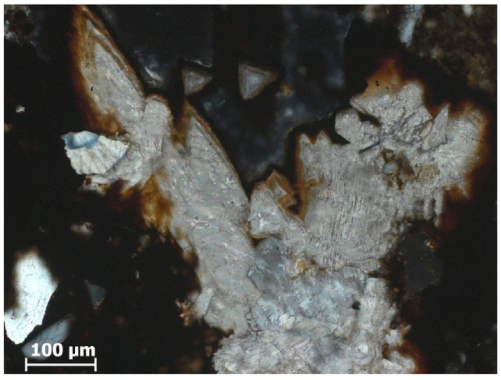
4.1.2.2. Micromorphological characteristics

4.1.2.2.1. 6Bg5 horizon (312–355 cm depth). The main *in situ* pedogenic processes identified in the thin section of this horizon are bioturbation (passage features and channels; Fig. 4a), *in situ* clay neoformation (indicated by stipple speckled b-fabric), and redoximorphosis as indicated by various kinds of nodules and hypocoatings showing irregular or diffuse outer boundaries that

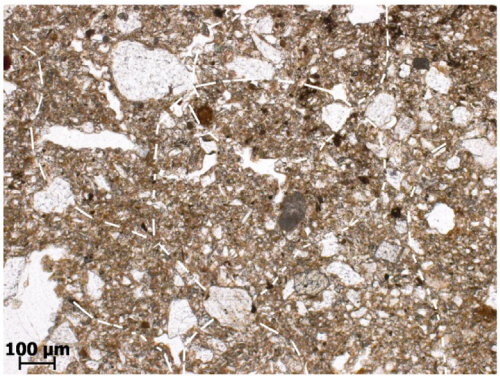
ARTICLE IN PRESS



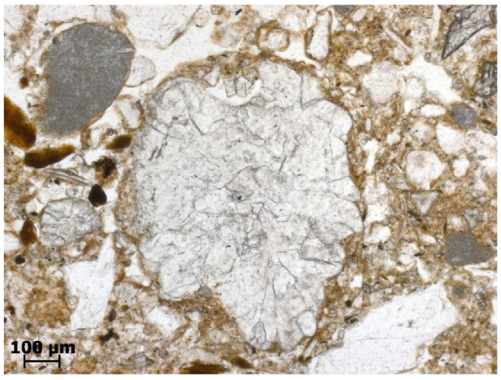
a) 6Bg5 (329-339 cm depth): Ferruginous concentric nodule – oblique incident light.



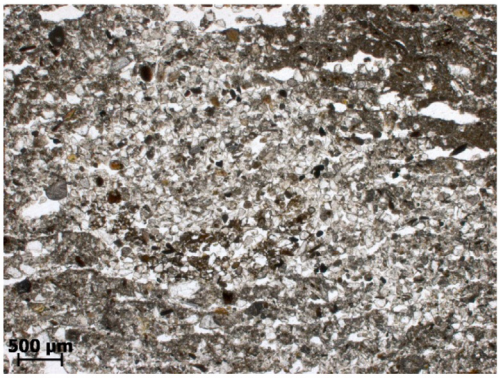
b) 6Bg5 (329-339 cm depth): Manganiferous ferruginous hypocoating on weathered dolomite – crossed polarizers.



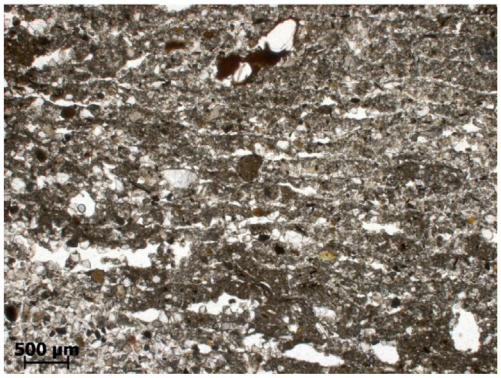
c) 5Bg4 (301-311 cm depth): Decarbonatised groundmass with micritic nodules and sparite in passage features (white circles) – plane polarised light.



d) 2Bg1 (202-212 cm depth): Biogenic calcite in the centre of the microphotograph. Micritic peloids of different size (e.g. one in the upper left corner) occur in the groundmass – plane polarised light.



e) Cg2 (163-173 cm depth): Silt infilling and lenticular platy microstructure; note that lenticular plates occur also in the filling. The fine-sandy to silty infilling has partly destroyed the original lenticular microstructure – plane polarised light.



f) Cg2 (163-173 cm depth): Lenticular platy microstructure with channels – plane polarised light.

Fig. 5. Micro-photographs of selected details of soil thin sections.

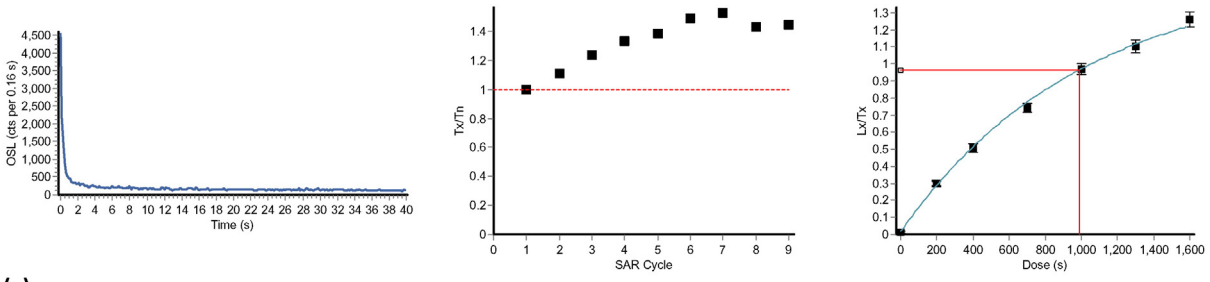
would not survive any transport (Fig. 5a, b). Coarse material that has been mixed in indicates lateral transport (sheet wash) prior to the final deposition of the reworked loess. Further details are provided in the supplementary material 4.

4.1.2.2.2. 5Bg4 (300–312 cm depth). The channel microstructure of this horizon, numerous fragments of mollusc shells, micritic nodules, sparite, biogenic calcites and passage features (Figs. 4b, 5c) indicate intense bioturbation by soil mesofauna. Again, coarse material that has been mixed in indicates lateral transport (sheet wash) prior to the final deposition of the reworked loess. The non-calcareous character of most of the finemass indicates decarbonatisation that was followed by clay neoformation (stipple speckled b-fabric). Another *in situ* soil-forming process is redoximorphosis as indicated by ferruginous concentric and aggregate nodules.

4.1.3. Soil-chemical and micromorphological characteristics of the Upper Pleniglacial (UPG) palaeosol horizons

4.1.3.1. Soil-chemical characteristics. Unexpectedly, also the lowermost UPG palaeosol horizons, namely the 2Bg1, 3Bw1 and 4Bg2 (190–275 cm depth; yellowish brown colour in Fig. 3) exhibit a rather intense brown colour and correspondingly high Fe_d/Fe_t ratios. The 3Bw1 and

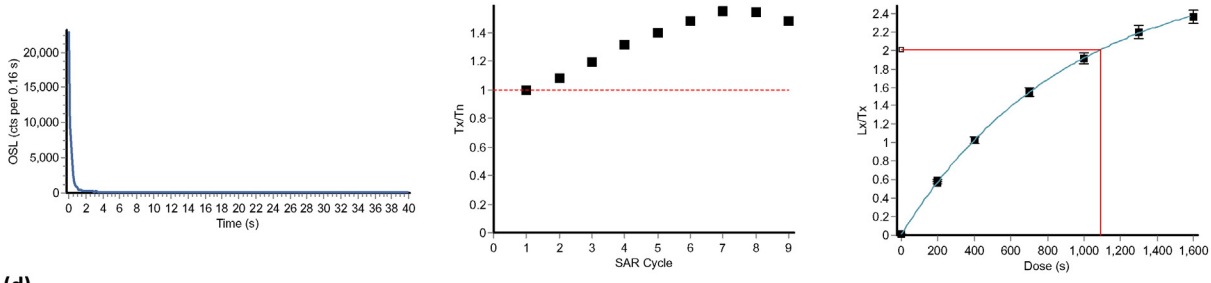
Please cite this article as: Sauer, D., et al., The loess-palaeosol sequence of Datthausen, SW Germany: Characteristics, chronology, and implications for the use of the Lohne Soi..., Catena (2016), http://dx.doi.org/10.1016/j.catena.2016.06.024



dose-recovery test HDS-1663, test-1, aliquot #18 (cf. Fig. S-2.2 in supplementary material 2):

- laboratory dose = ca. 95 Gy
- preheat-1 = 10 s at 240 °C
- preheat-2 = 10 s at 160 °C

- D_e = 988.84 ± 67.31 s
- recycling ratio = 0.99 ± 0.06 (run 7 / run 1)
- recuperation = 1.6 ± 0.4 % (run 8 / natural)
- BLSL counts ('natural') = 4529 cts (arbitrary units)
- BLSL counts (normalization dose 1000 s, run 1) = 5614 cts (a.u.)



SAR dating HDS-1663, measurement-1, aliquot #29:

- natural dose = unknown
- preheat-1 = 10 s at 240 °C
- preheat-2 = 10 s at 160 °C

- D_e = 1088.16 ± 65.69 s
- recycling ratio = 0.97 ± 0.04 (R 7/R 1)
- recuperation = 0.6± 0.1 % (run 8 / natural)
- BLSL counts ('natural') = 22818 cts (arbitrary units)
- BLSL counts (normalization dose 700 s, run 1) = 12226 cts (a.u.)

Fig. 6. Examples of SAR measurements of two aliquots with BLSL signals sufficiently bright for good D_e-determination. Sample HDS-1663 with D_e of ca. 1000 s (ca. 95 Gy). (a–c) Dose-recovery test. Test-1, aliquot #18 (cf. Fig. S-2.2 in Supplementary material 2). (d–f) Dated aliquot. Comparably bright BLSL signal. (a, d) Shine downs of first BLSL stimulation of SAR cycle (cf. run 1, set 4 in Table 3). (b, e) T_x/T_n curves recording sensitivity changes. (c, f) SAR dose-response curve with interpolated D_e (red line). (For interpretation of the references to colour in this figure legend, the reader is referred to the web version of this article.)

4Bg2 (220–275 cm depth; the 4Bg2 being the shallow horizon including the gravel layer that separates the UPG and MPG parts of the profile) exhibit Fe_d/Fe_t ratios as high as 0.35–0.36. These values equal those of the Bt horizon of the modern soil and the most intensively developed MPG palaeosol horizons (Fig. 3). The overlying 2Bg1 horizon (190–220 cm depth) has somewhat lower Fe_d/Fe_t ratios (0.32–0.34). In contrast to the MPG palaeosols, Mn_d/Mn_t ratios do not exceed Fe_d/Fe_t ratios in these three horizons (Fig. 3). The most probable explanation for this

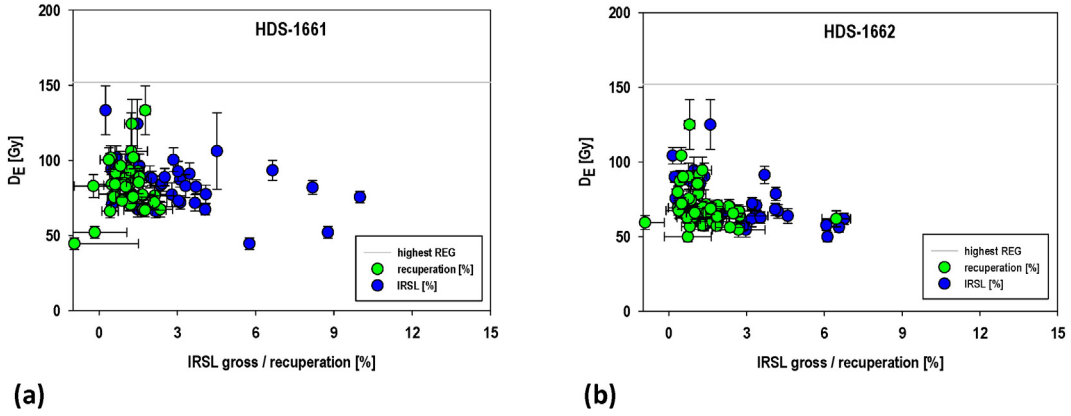


Fig. 7. D_e values versus proportion of the recuperated BLSL signal and the IRSL-signal for samples HDS-1661 (5Bg4, Lohne Soil, MPG part) and HDS-1662 (3Bw1, UPG part). Adjusted data sets with D_e values meeting the quality criteria (cf. Section 3.2.4) such as, e.g., ≤10 % recuperation and IRSL contribution as well as D_e being below the highest regeneration-dose point of ca. 150 Gy (cf. horizontal grey line). (For interpretation of the references to colour in this figure legend, the reader is referred to the web version of this article.)

Please cite this article as: Sauer, D., et al., The loess-palaeosol sequence of Datthausen, SW Germany: Characteristics, chronology, and implications for the use of the Lohne Soi..., Catena (2016), http://dx.doi.org/10.1016/j.catena.2016.06.024

ARTICLE IN PRESS

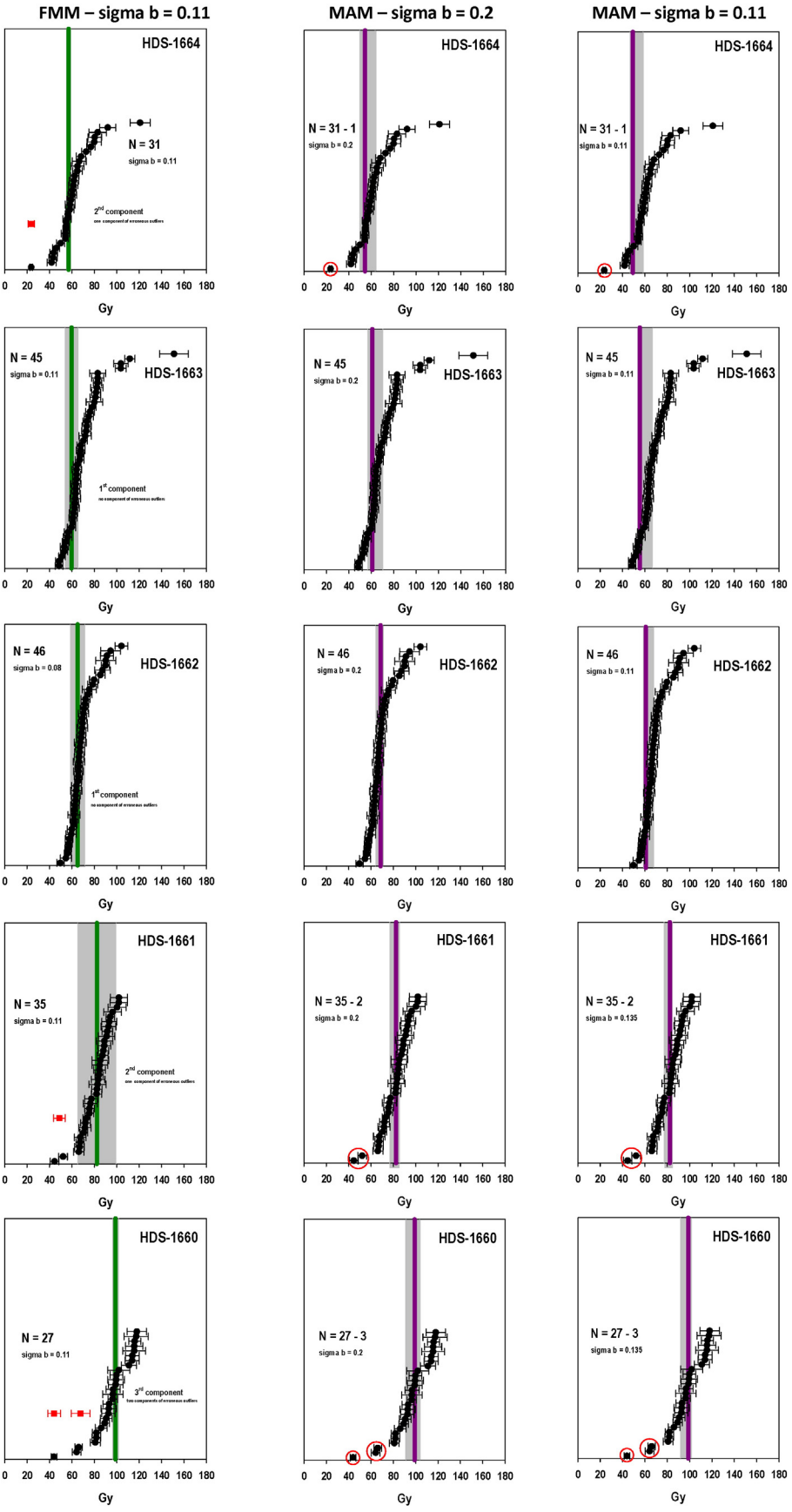


Fig. 8. Finite-mixture model (FMM; Galbraith, 2005) and minimum-age model (MAM; Galbraith et al., 1999) applied to the Datthausen samples. Sigma b of 0.2 (Arnold and Roberts, 2009) and 0.11 (Cunningham and Wallinga, 2012). Age modeling with the R package 'Luminescence' (Kreutzer et al., 2012b). Slight adaptations of sigma b were sometimes necessary for the software program to perform calculations. MAM ages calculated after eliminating outliers at the lower end (red circles). Agreement of results within error margins for all three approaches. (For interpretation of the references to colour in this figure legend, the reader is referred to the web version of this article.)

Please cite this article as: Sauer, D., et al., The loess-palaeosol sequence of Datthausen, SW Germany: Characteristics, chronology, and implications for the use of the Lohne Soi..., Catena (2016), http://dx.doi.org/10.1016/j.catena.2016.06.024

difference is that during the MPG period, when the channel was still deeper, additional Mn_d accumulated in the soils inside the channel through lateral Mn transport. This process seems likely because Mn is more redox-sensitive than Fe, and almost all palaeosol horizons show hydromorphic features (Table 1). This lateral Mn accumulation diminished as the channel was successively filled with sediment and thus became flatter and the concentration of lateral water flows inside the channel ceased.

Apart from the Fe_d/Fe_t ratios, all other data indicate less intense pedogenesis of the three lowermost UPG palaeosol horizons compared to the MPG palaeosol horizons. The SOC contents of the horizons 3Bw1 and 4Bg2 only amount to 0.13–0.17 %, those of the overlying 2Bg1 to 0.03–0.10 %. The calcium carbonate contents of the 3Bw1 and 4Bg2 amount to 12.4–13.9 % those of the overlying 2Bg1 horizon to 12.1–17.1 %. The WI_{MER} values of the 3Bw1 and 4Bg2 are 1.82–1.91 and those of the overlying 2Bg1 are 1.84–2.45, pointing to less extent of alkali and earth alkali element leaching compared to all MPG palaeosol horizons (having WI_{MER} values of 0.84–1.38). Such a combination of high Fe_d/Fe_t ratios and at the same time considerable carbonate content seems contradictory at first glance, since a precondition for the formation of significant amounts of pedogenic iron is previous decarbonatisation. Earlier decarbonatisation and subsequent recarbonatisation from overlying sediment can be excluded in this case, because no pedogenic carbonates were observed in the thin sections of the 3Bw1 and 2Bg1. The most probable explanation for the co-occurrence of high Fe_d/Fe_t ratios and remarkable carbonate contents is that the material contains some proportion of sediment that arrived in the channel already in a somewhat pre-weathered state and was mixed with non-decarbonatised loess during the transport into the channel. These layers, consisting of a mixture of fresh and pre-weathered material, were then subject to further *in situ* pedogenesis.

The three lowermost UPG palaeosol horizons characterised above are overlain by two hydromorphic palaeosol horizons, Cg1 and Cg2 (125–190 cm depth; grey colour in Fig. 3), showing the least stage of pedogenesis occurring in this profile. These two horizons have SOC contents of 0.12–0.14 % and calcium carbonate contents of 18.5–20.8 %, thus showing the least degree of decarbonatisation occurring in this profile. Their Fe_d/Fe_t ratios are 0.28–0.31 (Cg1) and 0.27 (Cg2), and their WI_{MER} values are as high as 2.54–2.86 (Cg1) and 2.93–2.94 (Cg2), respectively. Both, Fe_d/Fe_t ratios and WI_{MER} values thus identify the Cg2 as the least developed palaeosol horizon of the profile. This horizon has also the lowest clay/silt ratio (0.18) of all palaeosol horizons (Fig. 3). All other horizons exhibit greater clay/silt ratios, indicating various stages of clay formation, whereas in the Cg2 horizon hardly any pedogenic clay formation has taken place.

4.1.3.2. Micromorphological characteristics

4.1.3.2.1. 3Bw1 (220–260 cm depth). This horizon is characterised by a lenticular platy to compacted crumbly microstructure (Fig. 4c). Link cappings occur occasionally between lenticular plates. The lenticular platy microstructure has been partially destroyed by passage features that are abundant in this horizon (Fig. 4d). Hence, alternating freeze/thaw processes that created the platy structure must have preceded bioturbation. No decarbonatisation or re-carbonatisation is observed; thus the carbonate can be regarded as primary. Redoximorphic features are mostly *in situ*.

4.1.3.2.2. 2Bg1 (190–220 cm depth). This horizon is dominated by a weakly developed lenticular platy and crumbly microstructure. The abundance of passage features indicates nearly complete mixing of this horizon by soil mesofauna (Fig. 4e). The occurrence of biogenic calcite (Fig. 5d) and mollusc shells and the absence of secondary carbonates indicate that bioturbation took place in calcareous material. No decarbonatisation has taken place. Thus, a considerable proportion of the unusually intense brown colour of this horizon must be inherited from pre-weathered material. The occurrence of ferruginous concentric nodules is related to weak redoximorphic processes. Bioturbation and redoximorphic processes are *in situ* pedogenic processes. The passage features have not been altered by freeze/thaw processes. Apparently, such processes did not play an important role after the period of bioturbation, probably due to burial of the soil by enhanced sediment accretion. This interpretation is supported by the very low SOC concentrations in this horizon (Fig. 3). Usually, one would expect higher SOC concentrations in a horizon showing abundant bioturbation. Enhanced sediment accumulation rates may explain both, the absence of overprinting of the passage features by freeze/thaw processes and the low SOC contents of this horizon (due to dilution of SOC by the incoming sediment).

4.1.3.2.3. Cg2 (150–190 cm depth). This horizon has a lenticular platy microstructure, being a result of repeated freeze-thaw cycles. Most of the few passage features that are present (Fig. 4f) are related to a period prior to these freeze-thaw cycles, because they also have a lenticular platy microstructure (Fig. 5e), sometimes less developed because of a lower content of finemass. Primary carbonate is represented by finely dispersed micritic carbonate. Only slight secondary carbonatisation has taken place as indicated by weakly developed micritic hypocoatings.

Table 6
Results of the burial-dose (D_b) and minimum-age model (MAM) calculations.

Lab. No.	Depth [cm]	Horizon (FAO)	Effective dose rate [Gy ka^{-1}]	Minimum-age model (MAM) *		MAM age for sigma b = 0.2	
				Aliquots [N]	D_b for sigma b = 0.2 [Gy]	Age incl. error [ka]	Age span [ka]
HDS-1664	180	Cg2	2.50 ± 0.22	30	54.44 [− 4.67; + 9.04]	21.76 [− 2.65; + 4.08]	19.11 to 25.84
HDS-1663	216	2Bg1	2.68 ± 0.23	45	60.97 [− 4.17; + 9.32]	22.78 [− 2.49; + 3.99]	20.29 to 26.76
HDS-1662	245	3Bw1	2.64 ± 0.22	46	68.54 [− 4.45; + 2.18]	25.97 [− 2.76; + 2.34]	23.20 to 28.31
HDS-1661	297	5Bg3	2.95 ± 0.25	33	82.42 [− 5.56; + 3.00]	27.99 [− 3.03; + 2.58]	24.95 to 30.57
HDS-1660	333	6Bg5	2.81 ± 0.24	24	99.02 [− 7.72; + 4.41]	35.28 [− 4.06; + 3.37]	31.22 to 38.65

*MAM age (Galbraith et al., 1999) after elimination of outliers, sigma b = 0.2 (Arnold and Roberts, 2009).

Lab. No.	Depth [cm]	Horizon (FAO)	Effective dose rate [Gy ka^{-1}]	Minimum-age model (MAM) *		MAM age for sigma b = 0.11	
				Aliquots [N]	D_b for sigma b = 0.11** [Gy]	Age incl. error [ka]	Age span [ka]
HDS-1664	180	Cg2	2.50 ± 0.22	30	49.26 [− 2.52; + 8.95]	19.70 [− 1.98; + 3.96]	17.72 to 23.66
HDS-1663	216	2Bg1	2.68 ± 0.23	45	55.49 [− 2.11; + 11.35]	20.73 [− 1.93; + 4.59]	18.80 to 25.32
HDS-1662	245	3Bw1	2.64 ± 0.22	46	60.78 [− 2.17; + 6.96]	23.03 [− 2.11; + 3.27]	20.92 to 26.30
HDS-1661	297	5Bg3	2.95 ± 0.25	33	82.34 [− 5.09; + 2.21]	27.96 [− 2.93; + 2.48]	25.03 to 30.44
HDS-1660	333	6Bg5	2.81 ± 0.24	24	98.83 [− 7.05; + 3.08]	35.21 [− 3.90; + 3.18]	31.31 to 38.38

* MAM age (Galbraith et al., 1999) after elimination of outliers, sigma b = 0.11 (Cunningham and Wallinga, 2012).
** Ages of HDS-1660 and HDS-1661 were calculated using sigma b = 0.135 instead of sigma b = 0.11 (for software to perform calculation).

Please cite this article as: Sauer, D., et al., The loess-palaeosol sequence of Datthausen, SW Germany: Characteristics, chronology, and implications for the use of the Lohne Soi..., Catena (2016), http://dx.doi.org/10.1016/j.catena.2016.06.024

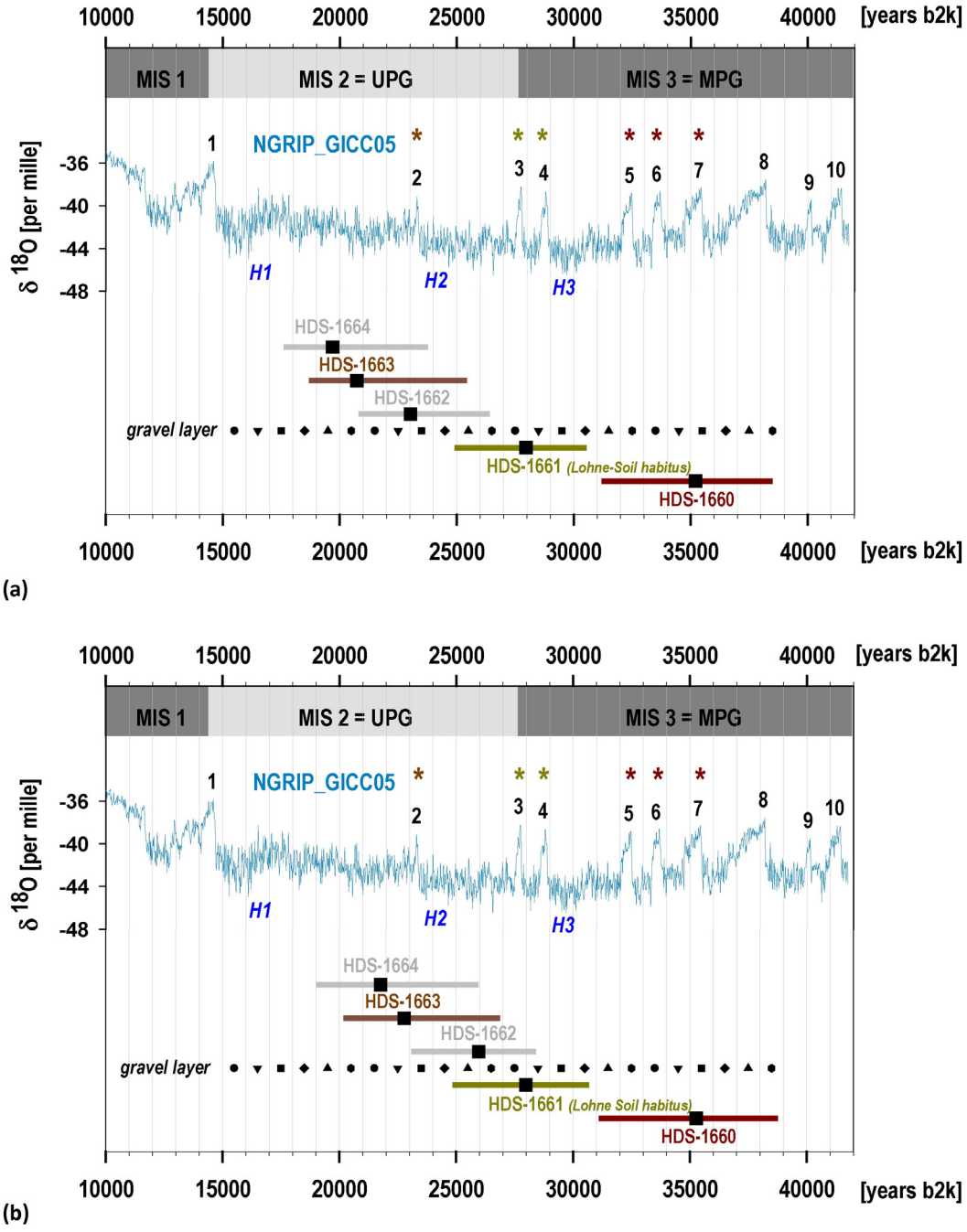


Fig. 9. BLSL-chronology for the loess section at Datthausen reflected in the Greenland Ice Core Chronology 2005 (GICC05). Data from the Centre for Ice and Climate/Niels Bohr Institute/University of Copenhagen: http://www.iceandclimate.nbi.ku.dk/; δ^{18}O-data are based on Dansgaard et al. (1993); GRIP Members (1993) and Johnsen et al. (1997). NGRIP with Greenland Ice Core Chronology 2005 (GICC05) (Andersen et al., 2006; Svensson et al., 2006) released 10 September 2007; file name 'GICC05_NGRIP_20y_10sep2007'; the NGRIP-data for the time-window of 10 to 42 ka are all from core NGRIP2 only. (a) MAM approach after elimination of outliers with sigma b = 0.11 (cf. Table 6, upper part). (b) Same as (a), but sigma b = 0.2 (cf. Table 6, lower part).

Some illuviation of clay from overlying horizons can be traced by dusty dark brown clay coatings (Fig. 5f). Both, the weak secondary carbonatisation and clay illuviation took place after the formation of the lenticular platy microstructure. Thus, the sequence of processes in this horizon is 1) activity of soil mesofauna, 2) enhanced influence of freeze-thaw cycles, 3) weak accumulation of secondary carbonates and illuvial clay from overlying horizons. Steps 1) and 2) took place when the soil horizon was still close to the surface. Step 3) took place later, after burial of the horizon Cg2. It is not part of the original pedogenesis of the Cg2 horizon but overprinted it.

4.2. OSL dating

4.2.1. Results of the equivalent dose (D_e) measurements

Application of the adapted SAR protocol (Section 3.2.4) to 64 aliquots per sample produced 27 (HDS-1660) to 46 aliquots (HDS-1662) per sample which met all quality criteria (cf. Section 3.2.5). An example of a SAR-dating measurement is given in Fig. 6d–f. The dating measurements showed similar behaviour as the dose-recovery measurements (Fig. 6a–c) supporting the reliability of the SAR protocol.

Please cite this article as: Sauer, D., et al., The loess-palaeosol sequence of Datthausen, SW Germany: Characteristics, chronology, and implications for the use of the Lohne Soi..., Catena (2016), http://dx.doi.org/10.1016/j.catena.2016.06.024

Fig. 7 illustrates the relationship between D_e values and the recuperated BLSL signal and the IRSL signal for aliquots with IRSL proportions below the threshold value of 10 %. Fig. 7a and b are examples of a sample from the MPG and UPG part of the profile, respectively, and confirm there is no dependency of D_e value on either of these criteria, and that the SAR protocol is reliable.

4.2.2. Burial dose (D_b) extraction

The accepted aliquots showed scattering D_e distributions with tails on the side of the larger values (Fig. 8 and Fig. S-5.1 in Supplementary material 5). As field investigations and micromorphological investigations suggested that the loess was reworked, the positive skewness of the D_e distributions was attributed to insufficient bleaching of the quartz grains prior to deposition. For such samples a minimum-age approach would provide the best estimate of the time of the last sediment deposition (Olley et al., 2004). This is a technique to extract the D_es of the best bleached aliquots from the population of aliquots and to calculate from that sub-population a representative burial dose (D_b) (Galbraith et al., 1999). The technique requires defining the class width (sigma b) which is equal to the overdispersion of a well-bleached sample. Sigma b values suggested in the literature range from 0.2 (Arnold and Roberts, 2009) to 0.11 (Cunningham and Wallinga, 2012). We applied both values for MAM age calculation. In some cases sigma b of 0.11 had to be changed slightly (0.08 to 0.135) as otherwise the software program could not have performed the calculation.

Three samples showed outliers at the lower end of the D_e distribution which cannot be explained by heterogeneous bleaching during the same depositional event. They represent erroneous ages which are not in agreement with the stratigraphy. This is best illustrated by sample HDS-1664 for which the aliquot with the lowest D_e of ca. 20 Gy would yield a Holocene age for the loess deposition. Such outliers are interpreted to result from post-depositional mixing in of mineral grains from overlying deposits. Therefore, we first applied a finite mixture model approach (Galbraith, 2005) to define the one or two of three components of aliquots which are assumed to represent the mixed-in grains. These were excluded from the population of aliquots which was regarded to represent the insufficiently bleached sediment as owed to the transport by water.

Results of the FMM and MAM approach are shown in Table 6 and Fig. 8. The extracted burial doses of a sample agree on the 1 sigma error level independent of the size of sigma b. Further, the results of the MAM approach after excluding the outliers at the lower end of the D_e distribution agree within error margins with the results of the FMM approach, i.e. the burial dose of the first FMM component for non-turbated samples (HDS-1662, HDS-1663) or the first component not interpreted to represent the burial dose of bio- or cryoturbated grains, i.e. component 2 for samples HDS-1661 and HDS-1664 and component 3 for sample HDS-1660 (see Supplementary material 5 for further details).

4.2.3. Obtained OSL ages and their interpretation

The obtained OSL ages are in stratigraphical order, becoming younger with decreasing depth (Fig. 9). As the suggestion for sigma b of 0.2 (Arnold and Roberts, 2009) is based on a larger data set than that for sigma b of 0.11 (Cunningham and Wallinga, 2012), we refer to the OSL ages based on the larger value for sigma b (Table 6, upper part; Fig. 9b). Unless otherwise noted, we do not consider an additional positive error, which one may consider for D_e underestimation during OSL dating (which is unlikely but possible; cf. dotted lines in Fig. S-2.9 of supplementary 2). The OSL ages comprise a time range between ca. 35 ka and ca. 22 ka. Thus the numeric dating meets the expectation that the Datthausen profile exhibits the MPG/UPG transition. It is important to keep in mind that OSL analyses denote the time when the sediment was last exposed to daylight. If one assumes that soil formation occurred during the Greenland interstadials (GIS) of the last Pleniglacial, this means that an OSL age corresponds to the cold period (Greenland stadial) preceding the GIS in which the palaeosol was formed.

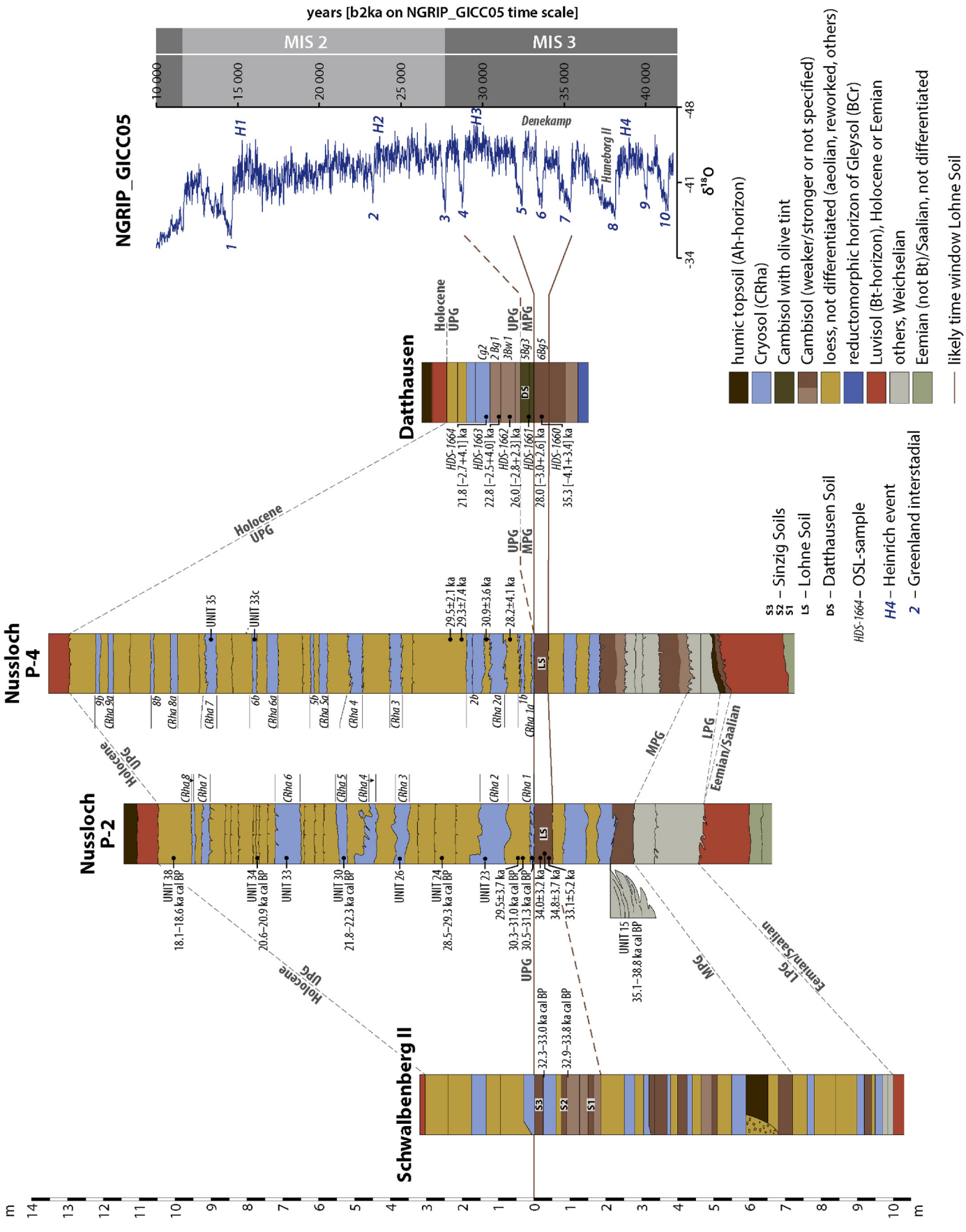
The lowermost dated OSL sample HDS-1660 from horizon 6Bg5 gave an age of 35.3 [−4.1, +3.4] ka which would conform with a period of soil formation during GIS 7 to GIS 5 (Fig. 9b). Thus, the period of formation of the most intensively developed palaeosol of the profile matches the period of the formation of the Lohne Soil and Sinzig Soils (S1 to S3) at Nussloch and Schwalbenberg II, respectively (Kadereit et al., 2013; Kadereit and Wagner, 2014).

OSL sample HDS-1661 from horizon 5Bg3 (showing Lohne Soil habitus) gave an age of 28.0 [−3.0, +2.6] ka (Fig. 9b). This time period could conform to soil formation during GIS 4 and/or GIS 3. Thus, the numerical dating suggests that the time of the terrestrial MPG/UPG transition conforms to the time of the MIS3/MIS2 transition in marine records. In contrast to Datthausen, the terrestrial MPG at Nussloch and Schwalbenberg II, marked by the Lohne Soil, appears to terminate already with the termination of GIS 5 (Kadereit et al., 2013). A younger IRSL age of the Lohne Soil at Nussloch (26.7 ± 3.4 ka) was attributed to reworking (Bibus et al., 2007). The observations from the Upper and Middle Rhine are in agreement with van Huissteden and Kasse (2001) and Vandenberghe (1995), who placed the MPG/UPG boundary at the termination of GIS 5, based on lithofacies changes in palaeofluvial environments in the Netherlands. The findings of an earlier beginning of the UPG in the loess-palaeosol profiles on the Upper and Middle Rhine are also in agreement with assumptions of comparably early Late Glacial Maximum (LGM) advances of the Scandinavian ice shield into northern Germany after ca. 34 ka (Lüthgens et al., 2011) and of the Inn glacier in the northern Alps in Austria ca. 32–33 ka ago (Spötl et al., 2013). The advances match the Greenland stadial between GIS 5 and GIS 4 and could be related to Heinrich 3 event (Spötl et al., 2013). Despite this accordance of the terrestrial record with independent proxies, age overestimation of the MPG/UPG boundary at Nussloch and Schwalbenberg II is possible. Likewise, age underestimation for samples HDS-1660 and HDS-1661 at Datthausen cannot be excluded. Mixing-in of quartz grains from younger layers may have led to age underestimation, despite the elimination of outlier D_es for burial-dose calculation (Section 4.2.2). In addition, the relatively large errors that are typical for OSL ages make unambiguous correlations between the terrestrial and the marine and ice-core archives impossible. However, also different palaeoenvironmental conditions at the Upper and Middle Rhine on the one hand and Datthausen on the other hand may have caused the later ending of MPG conditions at Datthausen. Nussloch and Schwalbenberg II represent sites that were directly exposed to sediment input from the nearby alluvial plain of the river Rhine acting as a huge source of dust, whereas the profile Datthausen received considerably less sediment. This becomes evident also when comparing the total thickness of the different profiles in Fig. 10.

The overlying OSL sample HDS-1662 from horizon 3Bw1 (representing the base of the UPG) gave an age of 26.0 [−2.8, +2.3] ka (Fig. 9b). This age appears to postdate GIS 3, thus corroborating the assumption that the terrestrial MPG/UPG boundary at Datthausen conforms to the MIS 3/MIS 2 boundary which matches the termination of GIS 3.

The overlying OSL sample HDS-1663 from horizon 2Bg1 gave an age of 22.8 [−2.5, +4.0] ka, suggesting a period of soil formation during GIS 2 (Fig. 9b). To our knowledge, the profile Datthausen is the first loess-palaeosol sequence in Germany that includes a palaeosol horizon reflecting considerable soil formation (beyond the formation of tundra Gleysols that are often observed in this stratigraphic position) possibly corresponding to GIS 2. This may be explained by the higher sedimentation rates in other loess-palaeosol sequences which dilute and thus possibly obscure pedogenesis during this period. However, we need to keep in mind that the intensive brown colour of this soil horizon is most likely only partially caused by autochthonous pedogenesis and partially by

Please cite this article as: Sauer, D., et al., The loess-palaeosol sequence of Datthausen, SW Germany: Characteristics, chronology, and implications for the use of the Lohne Soi..., Catena (2016), http://dx.doi.org/10.1016/j.catena.2016.06.024



Please cite this article as: Sauer, D., et al., The loess-palaeosol sequence of Datthausen, SW Germany: Characteristics, chronology, and implications for the use of the Lohne Soi..., Catena (2016), http://dx.doi.org/10.1016/j.catena.2016.06.024

pre-weathering (Section 4.1.3.1). Nevertheless, the horizon also showed traces of intense *in situ* bioturbation (Section 4.1.3.2).

The uppermost OSL sample HDS-1664 from horizon Cg2 gave an age of 21.8 [−2.7, +4.1] ka, thus falling into the Last Glacial Maximum (LGM). It appears to represent the time immediately subsequent to GIS 2 (Fig. 9b). Although error margins of the OSL ages allow only rough estimates of accumulation rates, a considerable difference in accumulation rates between the LGM part and the unit underneath is evident. The unit between 333 cm depth (HDS-1660) and 216 cm depth (HDS-1663) represents a time window of ca. 12 ka, corresponding to an accumulation rate of ca. 10 cm ka^{-1}. In contrast, the uppermost part above sample HDS-1664 (at 180 cm depth) represents a time window of supposedly only ca. 4 ka until the onset of Termination I (cf. Reitner, 2007) which would correspond to a 4–5 times higher accumulation rate during the LGM. Thus, the OSL ages of the profile Datthausen suggest that the Rhine glacier reached its maximum extension south of Datthausen ca. 22 ka ago. This conclusion is in agreement with *in situ* cosmogenic nuclide dating of the maximum LGM position of the piedmont lobe of the Aare-Rhone glacier in the western Alps (Ivy-Ochs et al., 2004, 2006, 2008).

5. Discussion and conclusions

5.1. The profile Datthausen compared to other loess-palaeosol sequences of Germany

5.1.1. Lower Pleniglacial (LPG)

Lower Pleniglacial palaeosols are completely missing in the profile Datthausen (Fig. 10). This is in agreement with three loess-palaeosol sequences studied by Kösel (2010) on terraces of Iller and Lech (tributaries to the Danube River) in the region between Biberach and Ulm, ca. 30–40 km east of the profile Datthausen. Either a sequence of early last-glacial palaeosols never existed in the upper Danube catchment due to a lack of loess accumulation, or the early last-glacial deposits have been widely eroded in the upper Danube-Iller-Lech region. As Kösel (1996: 88, 99f.) observed remnants of early last-glacial palaeosols in some sheltered locations in the region, the second explanation seems more likely.

5.1.2. Middle Pleniglacial (MPG)

One of the peculiarities of the profile Datthausen is the intense pedogenesis reflected in the MPG palaeosol horizons. It is interpreted to be the result of a low rate of loess accumulation, resulting in only minor dilution of the products of pedogenesis compared to thicker loess-palaeosol profiles like e.g. at Nussloch and Schwalbenberg II, where much higher rates of loess accumulation led to greater dilution and, in addition, to greater spreading of the MPG palaeosols and separation of the palaeosols formed in different periods of soil formation by layers of fresh loess. In contrast to this, in the profile Datthausen, several cycles of pedogenesis may have taken place in the same material because not much loess accumulated in colder, drier periods in between the soil formation cycles.

In addition to the effect of low loess accumulation rates, also the position of the profile inside a channel – where more moisture was available – should have contributed to the remarkable intensity of pedogenesis, especially during the MPG. The channel character of the location then decreased over time, as the channel was successively filled with reworked loess. Thus, the present surface soil has not developed in a channel position but on a level land surface; it does thus not benefit from additional moisture as did the palaeosols, especially the MPG palaeosols. The MPG palaeosols thus formed under cooler but moister conditions compared to the present-day soil. The interplay of these two opposing factors might explain the similarity of the Fe_d/Fe_t ratios of the MPG palaeosols and the present-day soil (Section 4.1.2.1).

A third effect that may have contributed to the particular pedogenesis at the profile Datthausen is texture. The reworked loess is characterised by rather high sand contents (Section 4.1.1), amounting to >25 % in most of the profile and up to 41 % in the Cg2 horizon. In contrast to this, Rhine loess at Schwalbenberg (Schirmer, 2012) contains <2 % sand. The high sand contents at Datthausen may have facilitated more rapid leaching of carbonates compared to other, siltier profiles. Thus, favourable conditions for enhanced weathering and brunification might have been reached more rapidly at Datthausen. The high sand contents are probably due to three reasons: (1) the profile Datthausen is close to the last-glacial Danube floodplain representing one of the sources of loess in the profile; and (2) the profile is located in a channel within the penultimate-glacial fluvioglacial terrace. Thus, repeated sediment influx from the higher surrounding areas into the channel by slope wash during the Last Glacial period is likely. At least occasionally, sand-size particles originating from the sandy-gravelly fluvioglacial terrace deposits may have been incorporated; (3) surface run-off (likely on frozen ground) that concentrated inside the channel led to relative enrichment of sand particles.

5.1.3. Upper Pleniglacial (UPG)

The profile Datthausen exhibits an UPG palaeosol horizon, 2Bg1 (Fig. 3), which most likely formed during GIS 2. This horizon is unusually intensively developed, although pre-weathering most likely contributed to some extent. This observation may demonstrate that, on the one hand, profiles characterised by low loess accumulation rates like the profile Datthausen do not provide high-resolution palaeoenvironmental records, but on the other hand, such profiles may enable the detection of phases of soil formation even during periods in which high-resolution profiles experienced such high rates of loess accretion that any pedogenic products in those profiles were too much diluted for detecting pedogenesis in the rapidly accumulating sediments. In this way, profiles like the profile Datthausen, may contribute complementary information to the one obtained from high-resolution loess-palaeosol sequences. Therefore, we suggest that future research should not focus entirely on high-resolution profiles but should also include sequences characterised by lower loess accumulation rates. A chance to also obtain palaeoenvironmental information from high-resolution profiles during periods of increased loess accumulation rates might be through biomarker composition and isotopy, which is not affected by the dilution effects mentioned above (Zech et al., 2013).

5.2. Suitability of the Lohne soil as pedostratigraphic marker

In the field work for this study, the bipartite olive-brown palaeosol and the overlying prominent erosional discontinuity were assumed to

Fig. 10. Simplified sketches of the loess sections Schwalbenberg II (after Schirmer, 2012), Nussloch (after Antoine et al., 2009) and Datthausen (cf. Fig. 2). Luminescence ages for Schwalbenberg II and Nußloch, 'age ± error' ka, 1 sigma, with reference to the year of publication; for Datthausen MAM approach with sigma b = 0.2 (cf. Fig. 9b, Table 6, upper part), age with asymmetric negative/positive error, 1 sigma, with reference to the year of publication. ^{14}C-age ranges 'age–age ka cal BP', 1 sigma, with reference to 1950 CE. Calibration CalPal-2007HULU, Weninger et al. (2012). NGRIP_CICC05 timescale after Andersen et al. (2006) and Svensson et al. (2006), with reference to 2000 CE. Nussloch presented with luminescence ages from around LS and ^{14}C-ages from samples evaluated as especially reliable by Antoine et al. (2009). Age range 38,750–35,130 a cal BP for thermokarst infilling (unit 15, after Antoine et al., 2009), which is stratigraphically below the Lohne Soil, based on ^{14}C-ages from ten wood samples matching time window for GIS 8 on NGRIP_CICC05 timescale ca. 38,300–35,500 a b2ka. MPG part of the terrestrial loess-palaeosol archives terminating most likely at Nussloch with a soil complex (LS; unit 20 after Antoine et al., 2001, 2009) corresponding to GIS 7 to GIS 5 (Kadereit et al., 2013) and at Schwalbenberg II with uppermost of three individually distinguishable palaeosols (S1–S3) with S2 corresponding to GIS 6 and S3 corresponding to GIS 5 (Kadereit and Wagner, 2014). MPG parts on the Upper and Middle Rhine thus apparently terminating at the termination of GIS 5 (cf. horizontal brown line at 0 m relative level). MPG-palaeosol formation on the upper Danube at Datthausen (DS, 5Bg3 and 5Bg4) possibly lasting until GIS 4/GIS 3 (cf. continuation of oblique dashed brown line). Figure modified and extended after Kadereit et al. (2013) and Kadereit and Wagner (2014). Cartography V. Schniepp.

Please cite this article as: Sauer, D., et al., The loess-palaeosol sequence of Datthausen, SW Germany: Characteristics, chronology, and implications for the use of the Lohne Soi..., Catena (2016), http://dx.doi.org/10.1016/j.catena.2016.06.024

represent the uppermost MPG and MPG/UPG transition. This preliminary interpretation was then confirmed by luminescence dating. Thus, the presence of this characteristic sequence allowed the establishment of a first stratigraphical framework already in the field, as it did in numerous previous studies. This preliminary stratigraphy was in turn an important prerequisite for selecting adequate positions for luminescence dating that aimed at narrowing down the time-span of the formation of the Lohne Soil and the subsequent erosional event. We therefore conclude that in loess-palaeosol studies in the humid region of central Europe the Lohne Soil may serve as a reliable *pedostratigraphic marker* and effective tool for stratigraphic orientation during field work, especially for discriminating UPG from MPG units.

5.3. Suitability of the Lohne Soil as chronometric marker

A *chronometric marker* should indicate a specific event and needs to possess a consistent chronometric position. However, different events take place over different time-spans. For instance, the deposition of a volcanic tephra is a matter of hours to a few days, whereas the formation of a soil horizon takes hundreds to thousands of years. Thus, we have to accept that *chronometric markers* do not necessarily indicate a short moment in time but often rather a period in time, especially if soil horizons are used as *chronometric markers*. Furthermore, with respect to the Lohne Soil, already since the first investigations, several authors assumed a multiple-phase development (e.g. Schönhals et al., 1964). Their conclusion was based on the diverse features observed in the Lohne Soil, pointing to different environmental conditions, including e.g. brunification under well-aerated conditions, redoximorphic Mn and Fe dynamics under temporarily water-logged conditions, and frost-thaw dynamics producing a fine platy structure. All of these features were observed in the horizons 5Bg3 and 5Bg4 of the profile Datthausen. Thus, the inherent characteristics of the Lohne Soil imply a longer time-scale allowing for climatic variation and periods in which soil formation may have been interrupted. Therefore, we need to discuss the maximum time-span that may be accepted for the formation of a *chronometric marker*. The answer to this question is not straight-forward but depends on the chronological resolution that is required by the research question of the respective study. In order to evaluate the impact of climate forcing on changes of terrestrial palaeoenvironments there is a general effort to compare loess-palaeosol sequences to high-resolution marine and ice-core records (cf. Figs. 9 and 10). In this context, a *chronostratigraphic marker sensu stricto* should represent not more than one climatic phase. Otherwise, it cannot add a useful contribution to the correlation between terrestrial and marine or ice-core records. Climatic phases may however have varying durations. Thus, it seems inappropriate to define the maximum time-span allowed for the formation of a *chronometric marker* in terms of absolute duration of its formation. Instead, we suggest the definition that a palaeosol that is to be used as a *chronometric marker sensu stricto* should be monogenetic, having formed during only one climatic phase. Soil formation of a *chronometric marker sensu stricto* should be continuous and uniform. Thus, only minor environmental shifts, not affecting the direction of soil formation to detectable degree, can be accepted within the climatic phase represented by a *chronometric marker sensu stricto*. The following exceptions from this rule may be allowed: 1) the marker palaeosol may also reflect the transition zones at the beginning and the end of the period that it represents, and 2) post-burial alteration, e.g., re-carbonatisation may be allowed.

If the research question requires a chronological resolution that allows for separation of different Greenland Interstadials – which is the case in many recent loess-palaeosol studies – a palaeosol horizon like the Lohne Soil that reflects several different climatic phases, probably corresponding to several Greenland Interstadials, cannot serve as a *chronometric marker*. On the other hand, if the research question does not require such high resolution, we can accept that a *chronometric marker* may comprise several Greenland Interstadials, provided that we know exactly, which particular Greenland Interstadials are comprised in such a *chronometric marker sensu lato*, and that the formation of the *chronometric marker sensu lato* took place in the same Greenland Interstadials in all profiles where it is identified.

In the case of the profile Datthausen, the most likely scenario is that the loess, in which the Lohne Soil formed, accumulated between GIS 5 and GIS 4 (Fig. 9b). Decarbonatisation and brunification occurred during GIS 4 and/or GIS 3. Hydromorphic overprinting of the Lohne Soil above a permafrost table and periglacial reworking of the upper horizon probably took place after GIS 3, possibly also during the cold period between GIS 4 and GIS 3.

The formation of the Lohne Soil at Nussloch and Schwalbenberg II most likely took place during the period between GIS 7 and GIS 5 (Kadereit et al., 2013). This time-span matches with the time of the formation of the intense brown palaeosol horizon 6Bg5 that is underlying the Lohne Soil in the Profile Datthausen. Therefore, we conclude that

1) several Greenland Interstadials provided suitable environmental conditions for the formation of soils with Lohne Soil habitus (GIS 4 to GIS 3 at Datthausen *versus* GIS 7 to GIS 5 at Nussloch);
2) soils with differing morphology formed in different places during the same Greenland Interstadials, depending on the respective site conditions (during GIS 7 to GIS 5: intense brown 6Bg5 horizon at Datthausen *versus* olive-brown Lohne Soil at Nussloch);
3) the Lohne Soil may still serve as a valuable *pedostratigraphic marker*; however, its suitability as a *chronometric marker* has been reduced over the last years by the continuously improving chronological resolution for the time-span of the terrestrial MPG/UPG transition. Compared to the increased chronological resolution that can nowadays be achieved for this period, the chronological position of the Lohne Soil in different profiles across the loess-covered region of humid central Europe is not specific enough to use the Lohne Soil as a *chronometric marker* in high-resolution environmental reconstructions based on loess-palaeosol sequences.

More research is needed to identify possible causes for the differences in pedogenesis that occur between different profiles for the same period of time. As demonstrated by the present-day soil distribution around the profile Datthausen (Fig. S-1.3/Supplementary material 1), spatial variability is not an exception but the rule. However, loess-palaeosol sequences are preserved only in limited patches, the palaeosols therein representing partly the regional environmental conditions and partly site-specific combinations of soil-forming factors. Thorough profile descriptions and analyses as well as high-resolution dating are required to separate the one from the other.

Supplementary data to this article can be found online at http://dx.doi.org/10.1016/j.catena.2016.06.024.

Acknowledgements

The authors were kindly supported by the following persons and institutions: Annerose Böttcher carried out the soil chemical and particle size analyses at the Soil Science Laboratories of the University of Hohenheim. Jutta Asmuth, with the help of Felizitas Wolf and Christopher Schultz, prepared and measured the OSL-samples in the Heidelberg Luminescence Laboratory. Volker Schniepp, assisted by Ulrich Selgert, prepared Figs. 1, 10 and S-1.1 (Supplementary material 1) at the University of Heidelberg; Fig. S-1.2 (Supplementary material 1) was prepared at the Regierungspräsidium Baden-Württemberg in Freiburg. We thank two anonymous reviewers whose valuable comments helped in improving the manuscript.

References

Adamiec, G., Heer, A., Bluszcz, A., 2012. Statistics of count numbers from a photomultiplier tube and its implications for error estimation. Radiat. Meas. 47 (9), 746–751.
Andersen, K.K., Svensson, A., Johnsen, S.J., Rasmussen, S.O., Biglera, M., Röthlisberger, R., Ruth, U., Siggaard-Andersena, M.-L., Steffensen, J.P., Dahl-Jensen, D., Vinther, B.M.,

Clausen, H.B., 2006. The Greenland Ice Core Chronology 2005, 15–42 ka. Part 1: constructing the time scale. Quat. Sci. Rev. 25, 3246–3257.
Antoine, P., Rousseau, D.-D., Zöller, L., Lang, A., Munaut, A.V., Hatté, C., Fontugne, M., 2001. High-resolution record of the last interglacial–glacial cycle in the loess palaeosol sequences of Nussloch (Rhine Valley — Germany). Quat. Int. 76 (77), 211–229.
Antoine, P., Rousseau, D.-D., Moine, O., Kunesch, S., Hatté, C., Lang, A., Tissoux, H., Zöller, L., 2009. Rapid and cyclic aeolian deposition during the Last Glacial in European loess: a high-resolution record from Nussloch, Germany. Quat. Sci. Rev. 28, 2955–2973.
Arnold, L.J., Roberts, R.G., 2009. Stochastic modelling of multi-grain equivalent dose (D_e) distributions: implications for OSL dating of sediment mixtures. Quat. Geochronol. 4, 204–230.
Bibus, E., 1974. Abtragungs- und Bodenbildungsphasen im Rißlöß. E & G Quat. Sci. J. 25, 166–182.
Bibus, E., Semmel, A., 1977. Stratigraphische Leithorizonte im Würmlöß des Mittelrhein-Gebietes. Geol. Jb. Hess. 105, 141–147.
Bibus, E., Frechen, M., Kösel, M., Rähle, W., 2007. Das jungpleistozäne Lößprofil von Nußloch (SW-Wand) im Aufschluss der Heidelberger Zement AG. E & G Quat. Sci. J. 56 (4), 227–255.
Brunnacker, K., 1954. Löß und diluviale Bildungen in Südbayern. E & G Quat. Sci. J. 4/5 (1), 84–86.
Cunningham, A.C., Wallinga, J., 2012. Realizing the potential of fluvial archives using robust OSL chronologies. Quat. Geochronol. 12, 98–106.
Dansgaard, W., Johnsen, S.J., Clausen, H.B., Dahl-Jensen, D., Gundestrup, N.S., Hammer, C.U., Hvidberg, C.S., Steffensen, J.P., Sveinbjörnsdottir, A.E., Jouzel, J., Bond, G., 1993. Evidence for general instability of past climate from a 250-kyr ice-core record. Nature 364, 218–220.
DTU Nutech, 2015. The Risø TL/OSL reader. http://www.nutech.dtu.dk/english/Products-and-Services/Dosimetry/Radiation-Measurement-Instruments/TL_OSL_reader.
Duller, G., 2013. Analyst, Version 4.10, Built 26 March.
Fink, J., 1956. Zur Korrelation der Terrassen und Lösse in Österreich. E & G Quat. Sci. J. 7, 49–77.
Frechen, M., Zander, A., Cilek, V., Ložek, V., 1999. Loess chronology of the last interglacial/glacial cycle in Bohemia and Moravia, Czech Republic. Quat. Sci. Rev. 18, 1467–1493.
Fuchs, M., 2001. Die OSL-Datierung von Archäosedimenten zur Rekonstruktion anthropogen bedingter Sedimentumlagerung. Geoarchäologische Untersuchungen im Becken von Phlious, NE-Peloponnes, Griechenland. Ibidem, Stuttgart (196 pp.).
Fuchs, M., Kreutzer, S., Rousseau, D.-D., Antoine, P., Hatté, C., Lagroix, F., Moine, O., Gauthier, C., Svoboda, J., Lisá, L., 2013. The loess sequence of Dolní Vestonice, Czech Republic: a new OSL-based chronology of the last climatic cycle. Boreas 42, 664–677.
Galbraith, R.F., 2005. Statistics for Fission Track Analysis. Chapman & Hall/CRC, Boca Raton.
Galbraith, R.F., Roberts, R.G., Laslett, G.M., Yoshida, H., Olley, J.M., 1999. Optical dating of single grains of quartz from Jinmium rock shelter, northern Australia. Part I: experimental design and statistical models. Archaeometry 41, 339–364.
Geyer, M., Nitsch, E., Simon, T., 2011. Otto F. Geyer/Manfred P. Gwinner: Geologie von Baden-Württemberg. (627 pp.)
Graul, H., 1952. Zur Gliederung der mittelpleistozänen Ablagerungen in Oberschwaben. E & G Quat. Sci. J. 2 (1), 133–146.
Greenland Ice-Core Project (GRIP) Members, 1993. Climate instability during the last glacial period recorded in the GRIP ice core. Nature 364, 203–208.
Guérin, G., Mercier, N., Adamiec, G., 2011. Dose-rate conversion factors: update. Ancient TL 29, 5–8.
Haase, D., Fink, J., Haase, G., Ruske, R., Pécsi, M., Richter, H., Altermann, M., Jäger, K.-D., 2007. Loess in Europe—its spatial distribution based on a European Loess Map, scale 1:2,500,000. Quat. Sci. Rev., 26, 1301–1312.
Haeserts, P., 1985. Les loess du Pléistocène supérieur en Belgique; comparaisons avec les séquences d'Europe Centrale. Bull. Assoc. Fr. Etude Quat. 2/3, 105–115.
Hambach, U., Zeeden, C., Veres, D., Obreht, I., Eckmeier, E., Fischer, P., Lehmkuhl, F., 2015. In: Mindrescu, M., Gradinaru, I. (Eds.), Towards mineral magnetic based millennial time scales in Late Pleistocene Danubian loess-palaeosol sequences. Abstract volume of the PAGES-supported meeting: Late Pleistocene and Holocene climatic variability in the Carpathian-Balkan region, held at Cluj-Napoca, Romania, 6–9 November 2014, Georeview. Scientific Annals of Stefan Cel Mare University of Suceava, pp. 67–71 Special Issue 2015.
IUSS Working Group WRB, 2014. World Reference Base for Soil Resources. World Soil Resources Reports. vol. 106 (Rome, 181 pp.).
Ivy-Ochs, S., Schäfer, J., Kubik, P.W., Synal, H.-A., Schlüchter, C., 2004. Timing of deglaciation on the northern Alpine foreland (Switzerland). Eclogae Geol. Helv. 97, 47–55.
Ivy-Ochs, S., Kerschner, H., Ruether, A., Maisch, M., Sailer, R., Schaefer, J., Kubik, P.W., Synal, H.-A., Schlüchter, C., 2006. The timing of glacier advances in the northern European Alps based on surface exposure dating with cosmogenic ^{10}Be, ^{26}Al, ^{36}Cl, and ^{21}Ne. Geol. Soc. Am. Spec. Pap. 415, 43–60.
Ivi-Ochs, S., Kerschner, H., Reuther, A., Preusser, F., Heine, K., Maisch, M., Kubik, P.W., Schlüchter, C., 2008. Chronology of the last glacial cycle in the European Alps. J. Quat. Sci. 23 (6–7), 559–573.
Johnsen, S.J., Clausen, H.B., Dansgaard, W., Gundestrup, N., Hammer, C.U., Andersen, U., Andersen, K.K., Hvidberg, C.S., Dahl-Jensen, D., Steffensen, J.P., Shoji, H., Sveinbjornsdottir, A.E., White, J., Jouzel, J., Fisher, D., 1997. The delta O18 record along the Greenland Ice Core Project deep ice core and possible Eemian climate instability. J. Geophys. Res. 102 (C12), 26397–26410.
Kadereit, A., Sponholz, B., Rösch, M., Schier, W., Kromer, B., Wagner, G.A., 2006. Chronology of Holocene environmental changes at the tell site of Uivar, Romania, and its significance for late Neolithic tell evolution in the temperate Balkans. Z. Geomorphol. N.F. Suppl.-vol. 142, 19–45.
Kadereit, A., Kind, C.-J., Wagner, G.A., 2013. The chronological position of the Lohne soil in the Nussloch loess section — re-evaluation for a European loess-marker horizon. Quat. Sci. Rev. 59, 67–86.
Kadereit, A., Kreutzer, S., 2013. Risø calibration quartz — a challenge for β-source calibration. An applied study with relevance for luminescence dating. Measurement 46 (7), 2238–2250.
Kadereit, A., Wagner, G.A., 2014. Geochronological reconsiderations for the eastern European key loess section at Stayky in Ukraine. Clim. Past Discuss. 9, 2629–2659.
Kösel, 1996. Der Einfluss von Relief und periglazialen Deckschichten auf die Bodenausbildung im mittleren Rheingletschergebiet von Oberschwaben. Tübinger Geowiss. Arb. D1 (147 p.).
Kösel, M., 2010. Zur Ausbildung von Lössen und Decklehmen auf den Deckenschottern des östlichen Rheingletschergebiets (Oberschwaben) und ihre Bedeutung für die Bodenverbreitung. LGRB-Inf. 25, 67–82.
Kreutzer, S., Fuchs, M., Meszner, S., Faust, D., 2012a. OSL chronostratigraphy of a loess-palaeosol sequence in Saxony/Germany using quartz of different grain sizes. Quat. Geochronol. 10, 102–109.
Kreutzer, S., Schmidt, C., Fuchs, M.C., Dietze, M., Fischer, M., Fuchs, M., 2012b. Introducing an R package for luminescence dating analysis. Ancient TL 30 (1), 1–8.
Lisiecki, L.E., Raymo, M.E., 2005. A Pliocene-Pleistocene stack of 57 globally distributed benthic δ^{18}O records. Paleooceanography 20, 1–17, PA1003. http://dx.doi.org/10.1029/2004PA001071 (Correction published 24 May 2005).
Litt, T., Behre, K.E., Meyer, K.-D., Stephan, H.-J., Wansa, S., 2007. Stratigraphische Begriffe für das Quartär des norddeutschen Vereisungsgebietes. E & G Quat. Sci. J. 56 (1/2), 7–65.
Lüthgens, C., Böse, M., Preusser, F., 2011. Age of the Pomeranian ice-marginal position in northeastern Germany determined by optically stimulated luminescence (OSL) dating of glaciofluvial sediments. Boreas 40, 598–615.
Marković, S.B., Hambach, U., Catto, N., Jovanovica, M., Buggle, B., Machalett, B., Zöller, L., Glaser, B., Frechen, M., 2009. Middle and Late Pleistocene loess sequences at Batajnica, Vojvodina, Serbia. Quat. Int. 198, 255–266.
Mehra, O.P., Jackson, M., 1960. Iron oxide removal from soils and clays by a dithionite-citrate system buffered with sodium-bicarbonate. Clay Clay Miner. 7, 317–327.
Müller, Ch, 2012. Geochronologische Untersuchungen zur Rekonstruktion der Landschaftsgeschichte zwischen Neckarschwemmfächer und Rheinterrasse seit dem letzten Hochglazial mittels optisch stimulierter Lumineszenzdatierung (thesis for the first state examination for high school teachers in Chemistry and Geography). Wissenschaftliche Arbeit für das erste Staatsexamen im Studiengang Lehramt für Gymnasium mit der Fächerverbindung Chemie/Geographie. University of Heidelberg 101 pp.
Murray, A.S., Wintle, A.G., 2000. Luminescence dating of quartz using an improved single-aliquot regenerative-dose protocol. Radiat. Meas. 32, 57–73.
Olley, J.M., Pietsch, T., Roberts, R.G., 2004. Optical dating of Holocene sediments from a variety of geomorphic settings using single grains of quartz. Geomorphology 60, 337–358.
Pécsi, M., Richter, G., 1996. Löss. Herkunft – Gliederung – Landschaften. Z. Geomorphol. N.F. (Suppl. 98) (Berlin, Stuttgart, 391 pp.).
Peticzka, R., Holawe, F., Riegler, D., 2010. Structural analyses on the modified paleosol sequence of "Stillfried B" with high resolution measurements of selected laboratory parameters. Quat. Int. 222, 168–177.
Reitner, J.M., 2007. Glacial dynamics at the beginning of termination I in the eastern Alps and their stratigraphic implications. Quat. Int. 164–165, 64–84.
Rousseau, D.-D., Wu, N., Pei, Y., Li, F., 2009. Three exceptionally strong east-Asian summer monsoon events during glacial times in the past 470 kyr. Clim. Past 5, 157–169.
Rousseau, D.-D., Antoine, P., Gerasimenko, N., Sima, A., Fuchs, M., Hatté, C., Moine, O., Zöller, L., 2011. North Atlantic abrupt climatic events of the last glacial period recorded in Ukrainian loess deposits. Clim. Past 7, 221–234.
Rousseau, D.-D., Ghil, M., Kukla, Sima, A., Antoine, P., Fuchs, M., Lagroix, F., Debret, Hatté, C., Moine, 2013. Major dust events in Europe during marine isotope stage 5 (130–74 ka): a climatic interpretation of the "markers". Clim. Past 9, 2213–2230.
Rusakov, A., Sedov, S., 2012. Late Quaternary pedogenesis in periglacial zone of northeastern Europe near ice margins since MIS 3: timing, processes, and linkages to landscape evolution. Quat. Int. 265, 126–141.
Sauer, D., Wagner, S., Brückner, H., Scarciglia, F., Mastronuzzi, G., Stahr, K., 2010. Soil development on marine terraces near Metaponto (Gulf of Taranto, southern Italy). Quat. Int. 222 (1–2), 48–63.
Schirmer, W., 2012. Rhine loess at Schwalbenberg II — MIS 4 and 3. E & G Quat. Sci. J. 61 (1), 32–47.
Schönhals, E., Rohdenburg, H., Semmel, A., 1964. Ergebnisse neuerer Untersuchungen zur Würmlößgliederung in Hessen. E & G Quat. Sci. J. 15, 199–206.
Schwertmann, U., 1964. Differenzierung der Eisenoxide des Bodens durch Extraktion mit Ammoniumoxalat-Lösung. Z. Pflanzenernaehr. Düngung Bodenkd. 105, 194–202.
Semmel, A., 1969. Bemerkungen zur Würmlößgliederung in Rhein-Main-Gebiet. Notizblatt des Hessischen Landesamts für Bodenforschung. Vol. 97, pp. 395–399.
Semmel, A., 1995. Ein Lößprofil bei Lisieux (Normandie) und seine stratigraphische Parallelisierung mit Würmlössen in Hessen. E & G Quat. Sci. J. 45, 59–61.
Semmel, A., 2009. Lohner Boden. Lithostratigraphic database of the German Stratigraphic Commission (LithoLex) (ID 1000008).
Smalley, I.J., Jefferson, I.F., Dijkstra, T.A., Derbyshire, E., 2001. Some major events in the development of the scientific study of loess. Earth Sci. Rev. 54 (1–3), 5–18.
Spötl, C., Reimer, P.J., Starnberger, R., Reimer, R.W., 2013. A new radiocarbon chronology of Baumkirchen, stratotype for the onset of the Upper Würmian in the Alps. J. Quat. Sci. 28, 552–558.
Svensson, A., Andersen, K.K., Bigler, M., Clausen, H.B., Dahl-Jensen, D., Davies, S.M., Johnsen, S.J., Muscheler, R., Rasmussen, S.O., Röthlisberger, R., Peder Steffensen, J., Vinther, B.M., 2006. The Greenland Ice Core Chronology 2005, 15-42 ka. Part 2: comparison to other records. Quat. Sci. Rev. Vol. 25 (Issue 23-24), 3258–3267.
Tamm, O., 1922. Eine Methode zur Bestimmung der anorganischen Komponenten des Gelkomplexes im Boden. Medd. Statens Skogsförsöksanstalt Vol. 19, pp. 385–404.

Please cite this article as: Sauer, D., et al., The loess-palaeosol sequence of Datthausen, SW Germany: Characteristics, chronology, and implications for the use of the Lohne Soi..., Catena (2016), http://dx.doi.org/10.1016/j.catena.2016.06.024

ARTICLE IN PRESS

Terhorst, B., Appel, E., Werner, A., 2001. Palaeopedology and magnetic susceptibility of a loess-palaeosol sequence in southwest Germany. Quat. Int. 76-77, 231–240.
Terhorst, B., Sedov, S., Sprafke, T., Peticzka, R., Meyer-Heintze, S., Kühn, P., Solleiro Rebolledo, E., 2015. Austrian MIS 3/2 loess-palaeosol records—key sites along a west-east transect. Palaeogeogr. Palaeoclimatol. Palaeoecol. 418, 43–56.
USGS, 2015. USGS EarthExplorer, 2015. SRTM Void Filled, 3 Arc-Second Data (90 m), Version 4.1 (http://earthexplorer.usgs.gov).
van der Hammen, T., 1995. The Dinkel valley revisited: pleniglacial stratigraphy of the eastern Netherlands and global climatic change. Med. Rijks Geol. Dienst. 52, 343–355.
van der Hammen, T., Maarleveld, G.C., Vogel, J.C., Zagwijn, W.H., 1967. Stratigraphy, climatic succession and radiocarbon dating of the last glacial in the Netherlands. Geol. Mijnb. 45, 33–35.
van Huissteden, J., 1990. Tundra rivers of the last glacial: sedimentation and geomorphological processes during the middle pleniglacial in Twente, eastern Netherlands. Med. Rijks Geol. Dienst. 44, 3–138.
van Huissteden, J., Kasse, C., 2001. Detection of rapid climate change in last glacial fluvial successions in the Netherlands. Glob. Planet. Chang. 28, 319–339.
Vandenberghe, J., 1995. Timescales, climate and river development. Quat. Sci. Rev. 14, 631–638.
Wagner, B., 2011. Spatial analysis of loess and loess-like sediments in the Weser-Aller catchment (Lower Saxony and northern Hesse, NW Germany). E &G Quat. Sci. J. 60 (1), 27–46.
Weninger, B., Jöris, O., Danzeglocke, U., 2012. CalPal-2007. Cologne Radiocarbon Calibration & Palaeoclimate Research Package (http://www.calpal.de/ (downloaded on 15 May 2012).
Zech, R., Zech, M., Marković, S., Hambach, U., Huang, Y., 2013. Humid glacials, arid interglacials? Critical thoughts on pedogenesis and paleoclimate based on multi-proxy analyses of the loess–paleosol sequence Crvenka, northern Serbia. Palaeogeogr. Palaeoclimatol. Palaeoecol. 387, 165–175.
Zöller, L., Semmel, A., 2001. 175 years of loess research in Germany — long records and "unconformities". Earth Sci. Rev. 54, 19–28.
Zöller, L., Oches, E.A., McCoy, W.D., 1994. Towards a revised chronostratigraphy of loess in Austria with respect to key sections in the Czech Republic and in Hungary. Quat. Sci. Rev. 13 (5–7), 465–472.
Zöller, L., Zöller, L., Richter, D., Masuth, S., Wunner, L., Fischer, M., Walpurga Antl-Weiser, W., 2013. Luminescence chronology of the Grub-Kranawetberg site, Austria. E & G Quat. Sci. J. 62 (2), 127–135.

Please cite this article as: Sauer, D., et al., The loess-palaeosol sequence of Datthausen, SW Germany: Characteristics, chronology, and implications for the use of the Lohne Soi..., Catena (2016), http://dx.doi.org/10.1016/j.catena.2016.06.024